

# **Structural Integrity of Water Reactor Pressure Boundary Components**

## **Progress Report Ending 29 February 1976**

F. J. Loss, Editor

*Thermostructural Materials Branch  
Engineering Materials Division*

August 26, 1976



**NAVAL RESEARCH LABORATORY**  
**Washington, D.C.**

### **NOTICE**

This report was prepared for the United States Nuclear Regulatory Commission, Office of Nuclear Regulatory Research under Contract AT(49-24)-0207. Neither the United States nor the United States Nuclear Regulatory Commission, nor any of their employees, nor any of their contractors, subcontractors, or their employees, makes any warranty, express or implied, or assumes any legal liability or responsibility for the accuracy, completeness or usefulness of any information, apparatus, product or process disclosed, or represents that its use would not infringe privately owned rights.

Distribution: NRC-1 and NRC-5

UNCLASSIFIED

UNCLASSIFIED

SECURITY CLASSIFICATION OF THIS PAGE (When Data Entered)

REPORT DOCUMENTATION PAGE		READ INSTRUCTIONS BEFORE COMPLETING FORM
1. REPORT NUMBER NRL Report 8006	2. GOVT ACCESSION NO.	3. RECIPIENT'S CATALOG NUMBER
4. TITLE (and Subtitle) STRUCTURAL INTEGRITY OF WATER REACTOR PRESSURE BOUNDARY COMPONENTS Progress Report Ending 29 Feb 1976		5. TYPE OF REPORT & PERIOD COVERED Progress report on a continuing NRL problem
		6. PERFORMING ORG. REPORT NUMBER
7. AUTHOR(s)  F.J. Loss, editor		8. CONTRACT OR GRANT NUMBER(s)
9. PERFORMING ORGANIZATION NAME AND ADDRESS  Naval Research Laboratory Washington, D.C. 20375		10. PROGRAM ELEMENT, PROJECT, TASK AREA & WORK UNIT NUMBERS  NRL Problem M01-40 Project AT(49-24)-0207
11. CONTROLLING OFFICE NAME AND ADDRESS U.S. Nuclear Regulatory Commission Division of Reactor Safety Research Washington, D.C. 20555		12. REPORT DATE August 26, 1976
		13. NUMBER OF PAGES 55
14. MONITORING AGENCY NAME & ADDRESS (if different from Controlling Office)		15. SECURITY CLASS. (of this report)  Unclassified
		15a. DECLASSIFICATION/DOWNGRADING SCHEDULE
16. DISTRIBUTION STATEMENT (of this Report)		
17. DISTRIBUTION STATEMENT (of the abstract entered in Block 20, if different from Report)		
18. SUPPLEMENTARY NOTES  This research was supported in part by the Department of the Navy, Office of Naval Research, Arlington, Va. 22217		
19. KEY WORDS (Continue on reverse side if necessary and identify by block number) Charpy-V test                      Precracked Charpy-V test Dynamic fracture toughness      Postirradiation properties recovery Fatigue crack propagation        Radiation sensitivity K <sub>Id</sub> Warm prestress Nuclear pressure vessel steels		
20. ABSTRACT (Continue on reverse side if necessary and identify by block number) This report describes progress in a program to characterize the properties and performance of materials with respect to the structural integrity of light-water reactor pressure boundary components. The work is sponsored primarily by the U.S. Nuclear Regulatory Commission. Studies on dynamic fracture toughness are also being conducted on a cooperative basis by the Electric Power Research Institute (EPRI) and NRL. In addition, the work on dynamic fracture toughness is supported by the Office of Naval Research. This report describes progress in the following areas: (a) fatigue crack propagation in reactor (Continues)		

DD FORM 1 JAN 73 1473

EDITION OF 1 NOV 65 IS OBSOLETE  
S/N 0102-014-6601UNCLASSIFIED  
SECURITY CLASSIFICATION OF THIS PAGE (When Data Entered)

UNCLASSIFIED

SECURITY CLASSIFICATION OF THIS PAGE(When Data Entered)

20. Abstract (Continued)

pressure vessel steels in an air environment, (b) dynamic fracture toughness of 1-in. (25-mm) and precracked Charpy-V bend specimens under impact loading, (c) postirradiation notch ductility and properties recovery in reactor vessel steels, (d) factors contributing to variable resistance of structural steels to radiation embrittlement, and (e) the initial program plan to investigate the phenomena of warm prestress and plastic net ligament in support of thermal shock studies.

UNCLASSIFIED

SECURITY CLASSIFICATION OF THIS PAGE(When Data Entered)

## CONTENTS

SUMMARY .....	iv
RESEARCH PROGRESS .....	1
I.    FATIGUE CRACK PROPAGATION IN LWR MATERIALS ...	1
A.    Comparisons of Crack Propagation in an Air Environment for A533-B Plate and A508 Forging and Weld Metal .....	1
II.   DYNAMIC FRACTURE TOUGHNESS .....	12
A.    Dynamic Toughness of 1-in. (25-mm) and Precracked Charpy-V Bend Specimens Under Impact Loading .....	12
B.    Further Analytical and Experimental Study of Inertial Loading in Notched Beam Impact Tests .....	23
III.  RADIATION SENSITIVITY AND POSTIRRADIATION PROPERTIES RECOVERY .....	28
A.    Low Fluence, 550° F (288° C) Radiation Assessment of Nuclear Reactor Vessel Steels Having Variable Copper Content .....	28
B.    Influence of Duplex Metallurgical Microstructure on Radiation Embrittlement Resistance of a Reactor Pressure Vessel Steel .....	31
IV.   THERMAL SHOCK-RELATED INVESTIGATIONS .....	35
A.    Initial Program Plan for Studies of Warm Prestress and Plastic Net Ligament Phenomena .....	35
REFERENCES .....	40
APPENDIX A — Procurement of A533-B and A302-B Steel Test Plates for Dynamic Fracture Toughness Studies .....	43

## SUMMARY

### I. FATIGUE CRACK PROPAGATION IN LWR MATERIALS

#### A. Comparisons of Crack Propagation in an Air Environment for A533-B Plate and A508 Forging and Weld Metal

Fatigue crack propagation trends are presented for A533-B plate, A508 Class 2 forging, and A508 submerged arc weld metal. The tests were conducted in a laboratory-air environment at 550° F (288° C) using 1-in. (25-mm) compact tension specimens. A modified trapezoidal waveform was used to cycle the specimens at 0.1 and 10 cpm. Comparison of the results from the plate, weld, and forging shows that the three materials exhibit similar trends in fatigue crack propagation for the test conditions investigated. The weld metal shows a somewhat higher growth rate than the plate or forging, and this rate exceeds that of the ASME Section XI crack growth curve for an air environment. For these tests, measurements of the crack length at the surface compared closely with crack length measurements made by means of the compliance method. Previous data indicate that tunneling of the crack front sometimes produces a significant difference between results from these two methods of crack length measurement. Contrary to tests conducted by others in a water environment, no increase in fatigue crack propagation was noted for these tests when the cyclic frequency was decreased to 0.1 cpm from 10 cpm.

### II. DYNAMIC FRACTURE TOUGHNESS

#### A. Dynamic Toughness of 1-in. (25-mm) Bend and Precracked Charpy-V Specimens Under Impact Loading

An experimental program is being conducted to characterize the dynamic fracture toughness of nuclear pressure vessel steels. Specific objectives are: (a) to characterize the dynamic initiation toughness ( $K_{Id}$ ) of three heats of pressure vessel steels, (b) to develop experimental and analytical techniques for the interpretation of notched, three-point bend specimen behavior under impact loading, and (c) to assess the validity of plane strain  $K_{Id}$  values as projected from the elastic plastic (J-Integral) analysis of smaller specimens. The  $K_{Id}$  vs temperature trends of the program materials have been characterized with precracked Charpy and 1-in. (25-mm) bend specimens loaded at the same rate ( $\dot{K}$ ). Whereas the results from both specimens agree at low temperatures, the precracked Charpy test appears to overestimate the toughness in the brittle/ductile transition region. An inconsistency for the 1-in. bend specimen has been noted between  $K_{Id}$  values computed from: (a) the fracture load, and (b) a J-Integral procedure using specimen energy to the time of fracture.

#### B. Further Analytical and Experimental Study of Inertial Loading in Notched Beam Impact Tests

An approximate theoretical analysis of the bending moments and the forces developed during impact of a notched beam in three-point bending has been completed. The elastic

analysis entails modeling the actual specimen as two smooth Timoshenko beams connected by a rotary spring. Use of Timoshenko beam theory makes it possible to include the effects of shear deflections and rotary inertia on the beam response. Initial calculations for a typical drop-weight impact test suggest that use of static analysis procedures (incorporating the hammer load directly) in the computation of stress intensity will, in general, lead to highly erroneous  $K_{Id}$  values. A series of experiments utilizing instrumented specimens is currently in progress to evaluate the analytical model.

### III. RADIATION SENSITIVITY AND POSTIRRADIATION PROPERTIES RECOVERY

#### A. Low Fluence, 550° F (288° C) Radiation Assessment of Nuclear Reactor Vessel Steels Having Variable Copper Content

A study of the low fluence, 550° F (288° C) radiation resistance of two reactor vessel steel types (A533-B and A302-B plates) and a representative reactor vessel weld deposit (A533-B, submerged arc weld) has been made using Charpy-V specimens. Copper contents of the materials were 0.3, 0.21, and 0.36%, respectively. Neutron fluence received by the samples was  $9.5 \times 10^{17}$  n/cm<sup>2</sup> > 1 MeV.

The radiation exposure was observed to produce a significant elevation in brittle/ductile transition temperature for the weld. Smaller increases in transition temperature were observed for the plates, consistent with their lower copper contents. None of the materials exhibited a degradation in Charpy-V upper shelf energy after irradiation. From this observation, NRC Regulatory Guide 1.99 would appear to be quite conservative in its projections of upper shelf energy degradation by low fluence. Good agreement, on the other hand, was noted between experimental measurements and Regulatory Guide 1.99 projections for low fluence, transition temperature behavior.

#### B. Influence of Duplex Metallurgical Microstructure on Radiation Embrittlement Resistance of a Reactor Pressure Vessel Steel

The relative influence of duplex upper bainite and ferrite microstructures vs fully upper bainitic microstructures on the radiation resistance of A302-B steel was explored, using Charpy-V specimens exposed to  $\sim 3.5 \times 10^{19}$  n/cm<sup>2</sup> at 550° F (288° C). The A302-B plates for the investigation were from 300-lb (135-kg) laboratory melts. One melt featured a "nominal" residual impurity element content patterned after the ASTM A302-B reference plate used in reactor vessel surveillance; the other melt represented a "low" impurity element content.

For the "nominal" residuals content material, no appreciable effect of microstructural type on radiation resistance was observed. On the other hand, a duplex microstructure did appear to be somewhat more radiation-sensitive for the case of a "low" impurity content. A limited assessment of 750° F (399° C) postirradiation heat treatment response to notch ductility is also described.

#### **IV. THERMAL SHOCK-RELATED INVESTIGATIONS**

##### **A. Initial Program Plan for Studies of Warm Prestress and Plastic Net Ligament Phenomena**

An experimental program is defined to quantify the effects of warm prestress and plastic net ligament behavior that may occur during the thermal shock of a nuclear pressure vessel following a main coolant pipe rupture and operation of the emergency core cooling system. By means of bend specimens of 1.5- and 3.0-in. (38- and 76-mm) thickness that were cut from A533-B Class 1 plate (HSST 02), the program will (a) demonstrate the effect of warm prestressing for enhancing the fracture toughness of A533-B steel when flawed material is subjected to a load and temperature history similar to that of the vessel wall during thermal shock, and (b) investigate crack propagation and arrest under conditions of limited displacement resulting in a plastic net ligament which simulates the behavior of a deep longitudinal crack during thermal shock. The results of this program will be used in the planning and interpretation of experimental thermal shock vessel tests being conducted by Oak Ridge National Laboratory.



**STRUCTURAL INTEGRITY OF WATER REACTOR  
PRESSURE BOUNDARY COMPONENTS  
PROGRESS REPORT ENDING 29 FEBRUARY 1976**

**RESEARCH PROGRESS**

**I. FATIGUE CRACK PROPAGATION IN LWR MATERIALS**

**A. Comparisons of Crack Propagation in an Air Environment  
for A533-B Plate and A508 Forging and Weld Metal**

H.E. Watson, F.J. Loss, and B.H. Menke

*Background*

Experimental results discussed here relate to fatigue crack propagation (FCP) tests conducted in air using A533-B plate, A508 Class 2 forging, and A508 submerged arc (S/A) weld metal (Table 1). These data are being developed as a base line reference for FCP studies at NRL of both irradiated and unirradiated material in a 550° F (288° C) reactor water environment. The FCP behavior of unirradiated material was characterized with 1-in. (25-mm) compact tension (CT) specimens at 550° F (288° C); a modified trapezoidal waveform with an R-ratio of 0.1 was used to cycle the specimens at frequencies of 0.1 and 10 cycles per minute (cpm). Crack extension was determined from both visual observation of one surface of the specimen and from either the average crack length measurements as defined by beach marks on the fracture surface or from an improved method for crack growth measurement, based on specimen compliance. The latter method was developed as part of the effort to permit automatic data accumulation and processing by computer. This method yields an average crack growth rate ( $da/dN$ ) similar to that determined from beach marks. In all cases reported here the  $da/dN$  values were determined by computer analysis using the incremental polynomial method recommended by the ASTM Task Group on Fatigue Crack Growth Rate Testing [1].

*Experimental Procedure*

The FCP data were generated using two 100 kip MTS servohydraulic machines operating under load control. Test parameters are defined in Table 2. Specimens were heated to 550° F (288° C) by an induction heating coil surrounding the specimen. This technique resulted in temperature uniformity within 20° F (11° C) throughout the specimen. The loading consisted of a modified trapezoidal waveform with an R-ratio nominally equal

to 0.1. The waveform consists of loading to maximum load at  $35$  to  $40 \times 10^3$  lb/s ( $156$  to  $178 \times 10^3$  N/s), holding at maximum load, then returning to minimum load at the same rate with no hold time at minimum load. For these experiments, surface crack extension was monitored by a closed circuit television system at 100X magnification. The progression of the crack length ( $a$ ) with cycles ( $N$ ) was periodically recorded by referencing engraved lines at 0.050-in. (1.3-mm) intervals on the specimen surface. These data were reduced using an HP 9830 computer to yield  $da/dN$   $\Delta K$  plots.

In each of the tests, beach marks on the fracture surface (Fig. 1) resulted because of varying degrees of oxidation. These beach marks define the tunneling of the crack front. Between five and ten well-defined lines were apparent, representing the true crack front shape at various times during testing. Crack length measurements at the 1/4, 1/2, and 3/4 thickness locations were made along each of these lines, and an average (quarter point) crack length was obtained. The number of cycles corresponding to each beach mark was determined from the intersection of the beach mark with the surface of the specimen. At this point the number of cycles corresponding to the surface crack was known from surface measurements described above. On the basis of these data a plot of  $a$  vs  $N$  was constructed and a smooth curve drawn through the points. The plots of  $da/dN$  vs  $\Delta K$  were constructed from the  $a$  vs  $N$  curve using the incremental polynomial method as recommended by the ASTM Task Group on Fatigue Crack Growth Rate Testing [1]. Since this method for computing  $da/dN$  requires more points than were available, additional points were assigned from the smooth curve. It is believed that the results obtained through this method produced no more error than would be introduced by taking arbitrary tangents ( $da/dN$ ) from the curve drawn through the values obtained from the beach marks.

The incremental polynomial method for determining  $da/dN$  involves the piecewise fitting, by least squares criteria, of seven consecutive data points,  $N_{i-3}$  to  $N_{i+3}$ , to a second order polynomial. This polynomial is differentiated to yield  $da/dN$  at the  $N_i$ th point.  $N_i$  is then incremented by one, and the process continues until all data points have been utilized. This method gives a result that is a smooth fit to the observed data and is suitable for computer processing.

An improved method for crack growth rate measurement, based on specimen compliance,\* was implemented: (a) in order to permit automatic data acquisition and processing by computer, and (b) to eliminate the necessity of relying upon measurement of crack propagation at the specimen surface. The compliance curve (Fig. 2) was determined from the linear slopes of load vs deflection lines from specimens having different machined-notch depths. The specimen deflection was monitored at the crack mouth by means of a high temperature clip gage.

During the conduct of the FCP test, the deflection of the clip gage is used to deduce the crack length by reference to the compliance calibration curve. Note that the compliance curve was determined from specimens having a machined crack front, whereas the test specimen has a fatigue crack with some degree of curvature. Consequently, the compliance method will yield the average crack length, which would normally be desired in an FCP test.

---

\*Specimen compliance is the inverse of the elastic spring constant of the material and can be expressed as the ratio of deflection/load ( $\delta/P$ ).

Table 1  
Material Chemistry and Heat Treatment

Material	Composition — wt %									
	C	Mn	P	S	Si	Ni	Cr	Mo	Cu	V
A-533B Class 1 HSST-01	0.22	1.37	0.008	0.008	0.22	0.66	0.15	0.54	0.18	0.02
A-508 Class 2 S/A Weld*	0.08	1.49	0.47	0.017	0.60	0.58	0.03	0.39	0.24	0.01
A-508 Class 2 Forging	0.19	0.69	0.007	0.009	0.31	0.82	0.38	0.62	0.01	0.13

Primary Heat Treatment

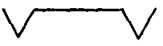
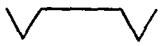

A-533 Class 1  
HSST-01  
Normalized at 1600°-1750° F (871-954° C) for 4 hours, air cooled; austenitized at 1500°-1650° F (816°-899° C) for 4 hours, quenched in agitated water; tempered at 1225° ± 25° F (663° ± 14° C) for 4 hours, furnace cooled.

A-508 Class 2  
S/A Weld  
Stress relief annealed at 1125° F (607° C) for 20 hours, furnace cooled.

A-508 Class 2  
Forging  
Austenitized at 1550° F (843° C) for 9 hours; water quenched; tempered at 1210° F (654° C) for 12 hours, air cooled; stress relief annealed at 1225° F (663° C) for 20 hours, furnace cooled at (55° F/hr max, 31° C/hr max).

\*Sub-arc Weld

Table 2  
Summary of Test Parameters

Material	Specimen No.	Frequency (cpm)	Loading Wave Shape	Ramp Rate (lb/s)	Hold Time (s)	R Ratio	Maximum Load (lb)	Specimen* Orientation
A533-B Class 1 (HSST-01 Plate)	L83-2	10.0		39,800	5.80	0.062	4,000	T-L
	L83-5	10.0		40,000	5.80	0.125	4,000	T-L
	L83-15	0.1		35,000	600.00	0.125	6,000	
A 508 Class 2 (S/A Weld)	Q93-10	10.0		35,000	5.80	0.125	4,000	†
	Q93-8	0.1		35,000	600.00	0.125	6,000	†
A 508 Class 2 (Forging)	Q71-3	10.0		35,000	5.74	0.125	5,250	C-L

\*Crack plane orientation codes are as specified in ASTM designation: E 399-72.

†Fatigue crack propagation in the welding direction plane of crack normal to the top surface

Note: All tests were in air at 550°F (288°C).

Metric conversion: lb/s × 4.48 = N/s



Fig. 1 — Typical beach marks on fracture surface of CT test specimen

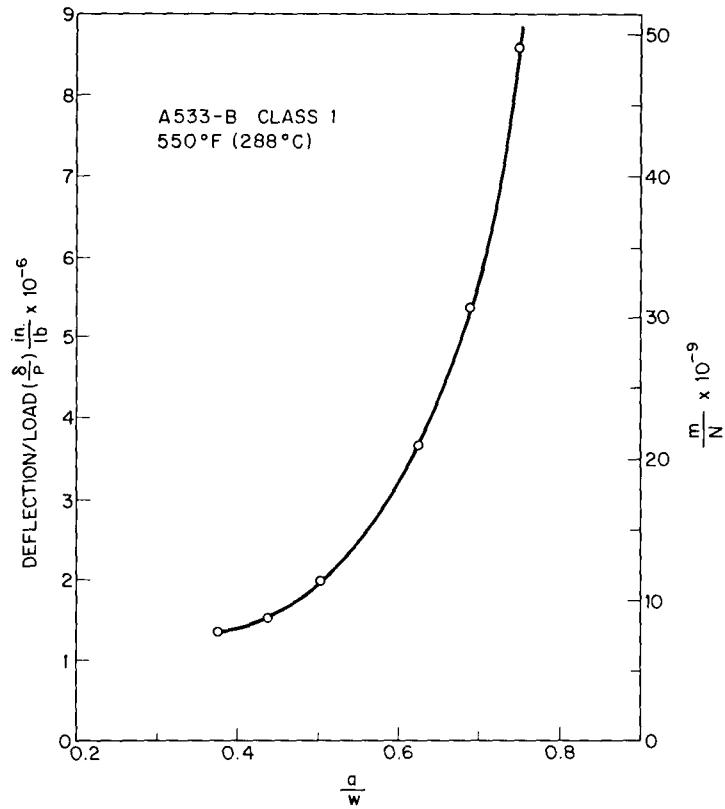


Fig. 2 — Compliance curve for A533-B Class 1 steel determined experimentally using specimens with notches machined to known depths

## NRL REPORT 8006

*Discussion*

Figure A-4300-1 of ASME Section XI [2] provides a curve intended to be an upper bound for fatigue crack propagation of subsurface flaws in an air environment. This curve is reproduced from the FCP data for the plate, weld, and forging materials presented in Figs. 3-8. It is believed that the Section XI curve is based largely on Westinghouse 2T WOL specimen test [3]. These tests were performed in a reactor water environment at 550°F (288°C), but at a cyclic rate (>60 cpm) considered to be too high to permit definition of environmental effects. The specimens were side grooved, which resulted in a relatively straight crack front.

On the other hand, tunneling was observed in the NRL tests. As a result, data from the 10-cpm tests (Figs. 3-6) suggest that the measurements from the specimen surface define a FCP rate greater than that determined from the average crack length as assessed from the beach marks. This impression is not entirely correct in that both the surface and beach mark data yield approximately the same crack growth rates as a function of *time* once the characteristic crack front geometry has been achieved. As a function of  $\Delta K$ , however, the  $da/dN$  values determined by the beach mark technique appear to fall below those determined from surface measurements. This apparent decrease in growth rate determined from beach marks is due to tunneling of the crack front (Fig. 1), a process that produces a longer average crack length, and therefore, a larger value of  $\Delta K$ . For example, a difference of up to 0.090 in. (2.3 mm) in crack length between the surface and mid-thickness locations resulted in a variation in  $\Delta K$  of 13 ksi $\sqrt{\text{in.}}$  (14.3 MPa $\sqrt{\text{m}}$ ) when surface or average crack lengths were used in the calculations.

The data from the 0.1 cpm tests (Figs. 7,8) show no differences between FCP rates determined from the surface of the specimen and those determined from the compliance method. The specimens used to generate the data presented in Figs. 7,8 showed only a small degree of tunneling compared with the specimens documented in Figs. 3-6. Consequently, a difference in data trends is not expected in results obtained by the surface and compliance methods.

Since the degree of crack tunneling for a given specimen cannot be reliably predicted, it is concluded that a standard method of reporting FCP data should be developed. The compliance method is an obvious choice for this purpose in that it provides a measure of the average crack growth rate, which, in turn, is believed to be more useful for describing specimen behavior than the surface crack method would be.

The 10-cpm data (Figs. 3-6) from surface measurements and beach mark measurements are plotted in Figs. 9 and 10, respectively, and comparisons are made with the Section XI curve. All the materials exhibit essentially similar crack growth rates, but the weld metal shows the highest growth rate. The data from surface measurements, Fig. 9, show that the Section XI line is exceeded by all the material, whereas only the weld metal exceeds the Section XI curve on the basis of beach mark measurements (Fig. 10). The data in Fig. 10 (with the exception of the weld metal) are similar to the Westinghouse data [3] upon which the Section XI curve is based.

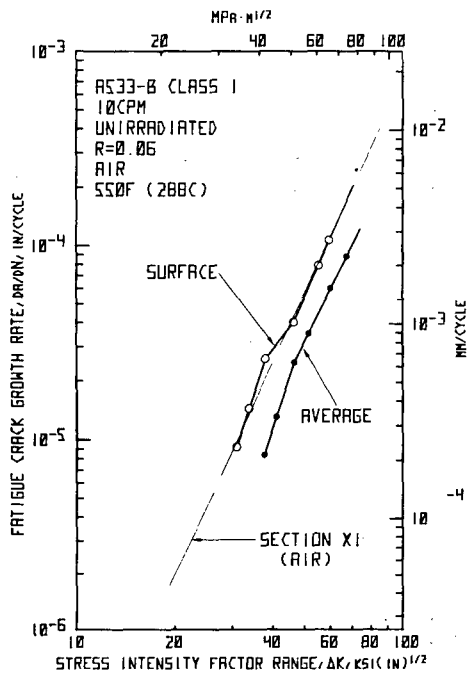


Fig. 3 — Crack growth rate data for A533-B plate obtained from surface crack length measurements and beach mark (average) referenced to the ASME Section XI upper bound fatigue crack growth rate curve

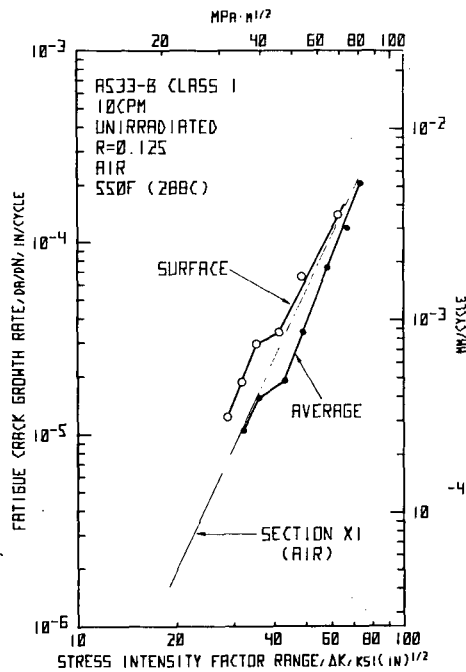


Fig. 4 — Crack growth rate data for A533-B plate obtained from surface crack length measurements and beach mark (average) referenced to the ASME Section XI upper bound fatigue crack growth rate curve



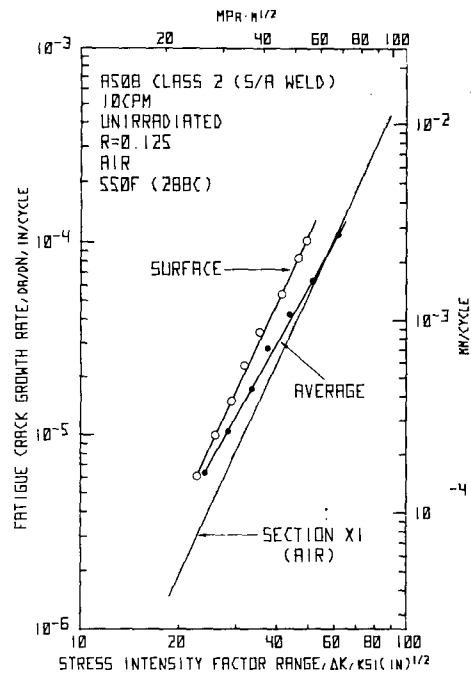


Fig. 5 — Crack growth rate data for A508 submerged arc weld metal material obtained from surface crack length measurements and beach mark (average) referenced to the ASME Section XI upper bound fatigue crack growth rate curve

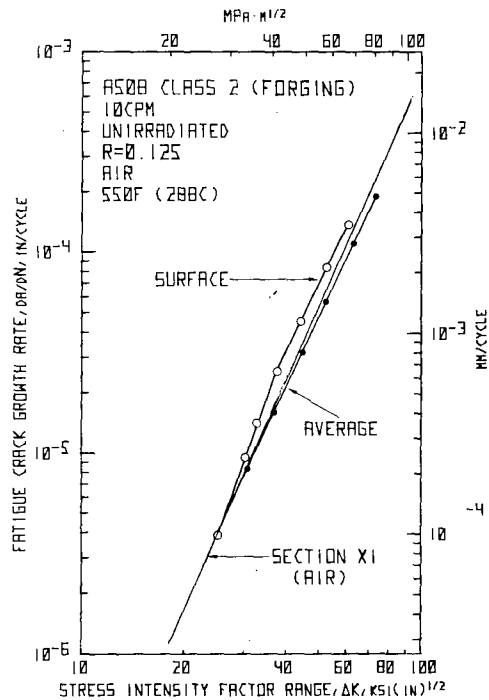


Fig. 6 — Crack growth rate data obtained for A508 forging from surface crack length measurements and beach mark (average) referenced to the ASME Section XI upper bound fatigue crack growth rate curve

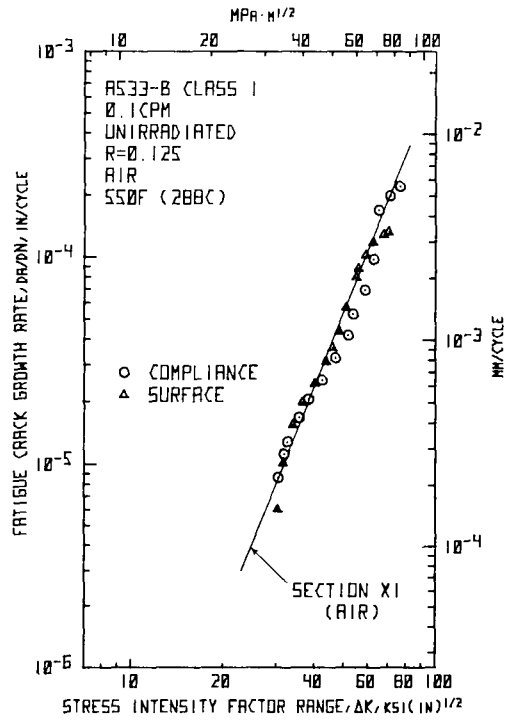


Fig. 7 — Crack growth rates in A533-B steel cycled at 0.1 cpm as determined by surface and compliance techniques

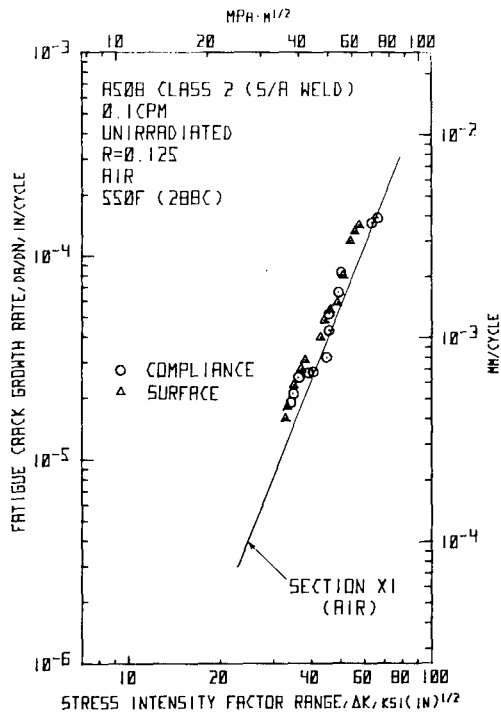


Fig. 8 — Comparison of crack growth rates in A508 submerged arc weld metal cycled at 0.1 cpm as determined by surface and compliance techniques

## NRL REPORT 8006

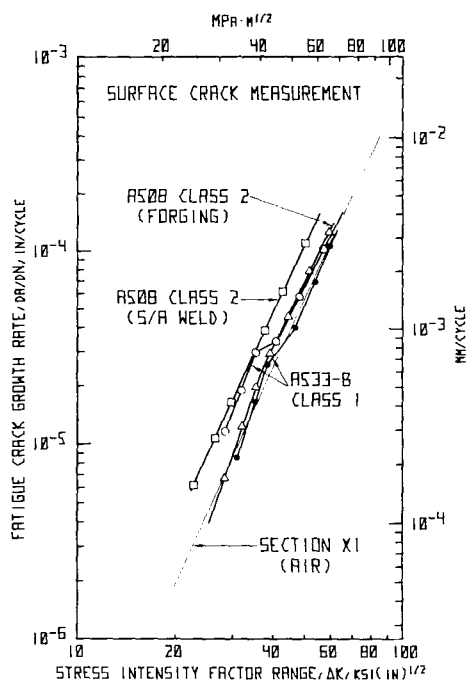


Fig. 9 — Fatigue crack growth data in air at 10 cpm obtained from surface crack length measurements compared with the ASME Section XI upper bound fatigue crack growth curve. Surface data indicate growth rates higher than the upper bound curve.

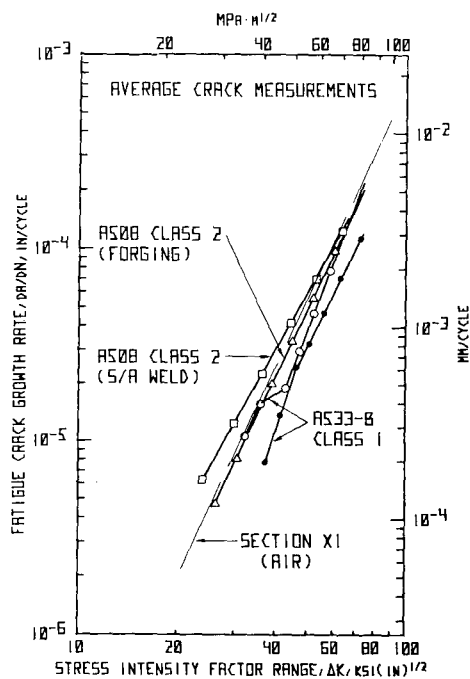


Fig. 10 — Fatigue crack growth data in air at 10 cpm obtained from beach mark (average) crack lengths compared with the ASME Section XI upper bound fatigue crack growth curve. Beach mark data indicate growth rates below the Section XI curve with the exception of the weld metal.

A comparison of the 10-cpm to the 0.1-cpm data is made in Figs. 11 and 12 for the plate and forging materials, respectively. Note that no apparent difference exists as a result of a decrease in the cyclic rate from 10 cpm to 0.1 cpm. This result is contrary to the data of Gerber et al [4] which show a pronounced increase in FCP rate in a water environment when the cyclic frequency is reduced. This suggests that a water environment is required in order to obtain FCP representative data for an LWR pressure vessel.

### *Conclusions*

Comparison of results from plate, weld, and forging shows that the three materials exhibit similar trends in FCP for the test conditions involved (Table 2), with the weld metal showing a somewhat higher growth rate than the plate or forging. The growth rates for both the plate and weld materials in air did not increase with a lower cyclic frequency (0.1 vs 10 cpm), contrary to results observed by others in a water environment. On the basis of beach marks, the crack growth rates appear to be in good agreement with similar data generated by Westinghouse in both air and water environments. The latter data were obtained at high cyclic rates ( $\geq 60$  cpm), where the environment is not believed to influence the crack growth behavior. Both Westinghouse and NRL beach mark data lie close to the ASME Section XI [2] upper bound fatigue crack growth curve for an air environment. An exception to this is the weld metal, which exhibits a crack growth rate somewhat in excess of the Section XI curve. A comparison of crack growth rates determined by surface measurements with those determined by means of beach marks or compliance shows the surface measurement method sometimes produces a fictitiously high growth rate that is in excess of the Section XI curve and depends on the degree of crack front curvature. This phenomenon points out the need to develop a standardized (interlaboratory) method for the reporting of FCP data.

## II. DYNAMIC FRACTURE TOUGHNESS

### A. Dynamic Toughness of 1-in. (25-mm) and Precracked Charpy-V Bend Specimens Under Impact Loading

F.J. Loss, J.R. Hawthorne, C.A. Griffis, and R.A. Gray

#### *Background*

The current program involves an investigation of the dynamic fracture toughness of nuclear pressure vessel steels. This research is sponsored by NRC but also represents a cooperative effort between NRL and the Electric Power Research Institute (EPRI). The principal objectives are: (a) to characterize the dynamic fracture initiation toughness ( $K_{Id}$ ) of three heats of LWR pressure vessel steel, (b) to develop experimental and analytical techniques for the interpretation and analysis of notched, three-point bend specimen behavior under impact loading, and (c) to assess the validity of plane strain  $K_{Id}$  values as projected from the elastic plastic (J-Integral) analysis of smaller specimens.

## NRL REPORT 8006

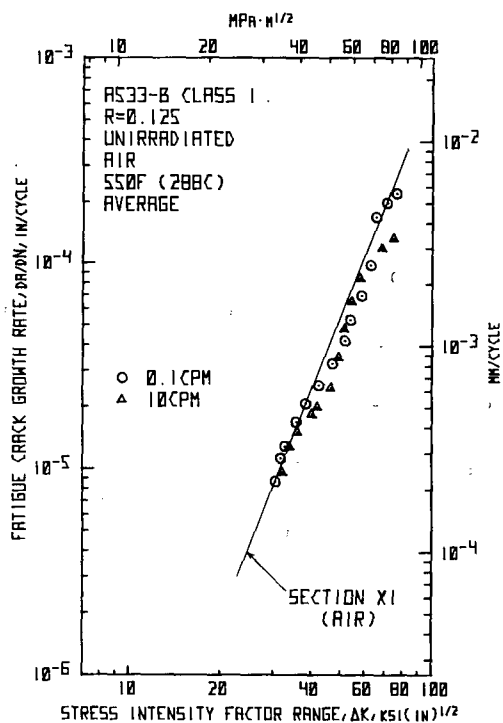


Fig. 11 — Assessment of the effect of cycling rate (0.1 and 10 cpm) on fatigue crack growth rate of A533-B steel in an air environment

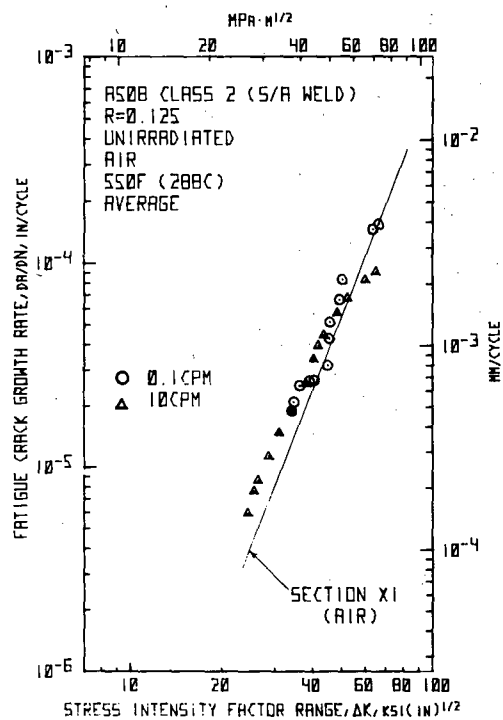


Fig. 12 — Assessment of the effect of cycling rate (0.1 and 10 cpm) on fatigue crack growth rate of A508 submerged arc weld metal in an air environment

The experimental program includes three pressure vessel steels, namely: 8-in. (203 mm) A533 Class 1 plate, 6-in. (152 mm) A302-B plate, and 9-in. (229 mm) A508 Class 2 forging. A fourth pressure vessel material, 4-in. (102 mm) A212-B plate, was added for initial experiments to conserve the program material. The first two plates were purchased to provide material representative of current and early vessel construction, respectively, and in sufficient quantity to meet the large-size specimen requirements. The melt for the A302-B plate was specially selected and processed in an attempt to provide a 50-ft-lb (68-J) Charpy-V ( $C_v$ ) upper shelf energy; this energy is the lowest value permitted in conjunction with the  $K_{IR}$  procedures of the ASME Code. The acquisition of low shelf material will permit an evaluation of: (a) the elastic plastic behavior in the ductile/brittle transition regime by J-Integral methods, and (b) the significance of low  $C_v$  upper shelf toughness in thick sections by advanced experimental methods. The material in the latter case also would simulate, in part, low  $C_v$  upper shelf toughness produced by irradiation. Purchase specifications, chemical composition, and heat treatments for the A533-B and A302-B plates are given in Appendix A. Properties for the A508 Class 2 and A212-B materials are presented in Ref. 5.

Three-point, notched bend specimens and a drop-weight test mode are employed because of: (a) versatility with respect to specimen geometry and loading rate variations without requiring major testing machine modifications, (b) the ability to achieve loading rates ( $\dot{K}$ ) above those obtainable on most closed-loop hydraulic machines, and (c) the similarity to the  $C_v$  and precracked  $C_v$  (PCC $_v$ ) specimens used in reactor vessel surveillance programs. Large specimens, up to 6-in. (152-mm) thickness, are included to provide the mechanical constraint necessary to "track" the toughness into the region of sharply increasing  $K_{Id}$  with increasing temperature. These results should provide the basis for assessing the validity of  $K_{Id}$  values projected from smaller specimens (PCC $_v$  and 1-in. (25 mm) bend) that exhibit elastic plastic behavior in the same temperature regime.

### *Dynamic Tear Test Evaluations*

Because specimen thicknesses up to 6 in. are involved in the fracture toughness testing program, good uniformity of properties through the thickness is essential to the testing plan. A program is being conducted to assess property gradients in these materials; included are tensile, drop-weight, and dynamic tear (DT) tests. Data concerning these properties are provided in Ref. 5 for the A508 Class 2 forging.

DT tests of the A302-B and A533-B Class 1 plate were recently completed. Results are reported in Figs. 13 and 14. The 5/8-in. (16-mm) thick specimens were oriented in the transverse (TL) test direction and were taken from the plate thickness locations indicated by the insert diagram. The plate surface designated as "top" was arbitrarily chosen in each case. The results for both plates show a good uniformity in properties for all but a thin 3/4-in. (19-mm) max. layer at each surface. For the A302-B plate, the data for the two surface layers themselves are in good agreement. For the A533-B plate on the other hand, the brittle/ductile transition of the bottom surface is significantly lower than that of the top surface. At a depth of only 5/8 in. into the plate, however, this difference no longer exists, as evidenced by the agreement of the half-filled circle and square symbol data points. Moreover, the plate exhibits the beginning of through thickness uniformity in properties at this depth. In summary, the DT data for both plates indicate that they are free of deleterious notch toughness gradients in the primary region of interest (thickness).

## NRL REPORT 8006

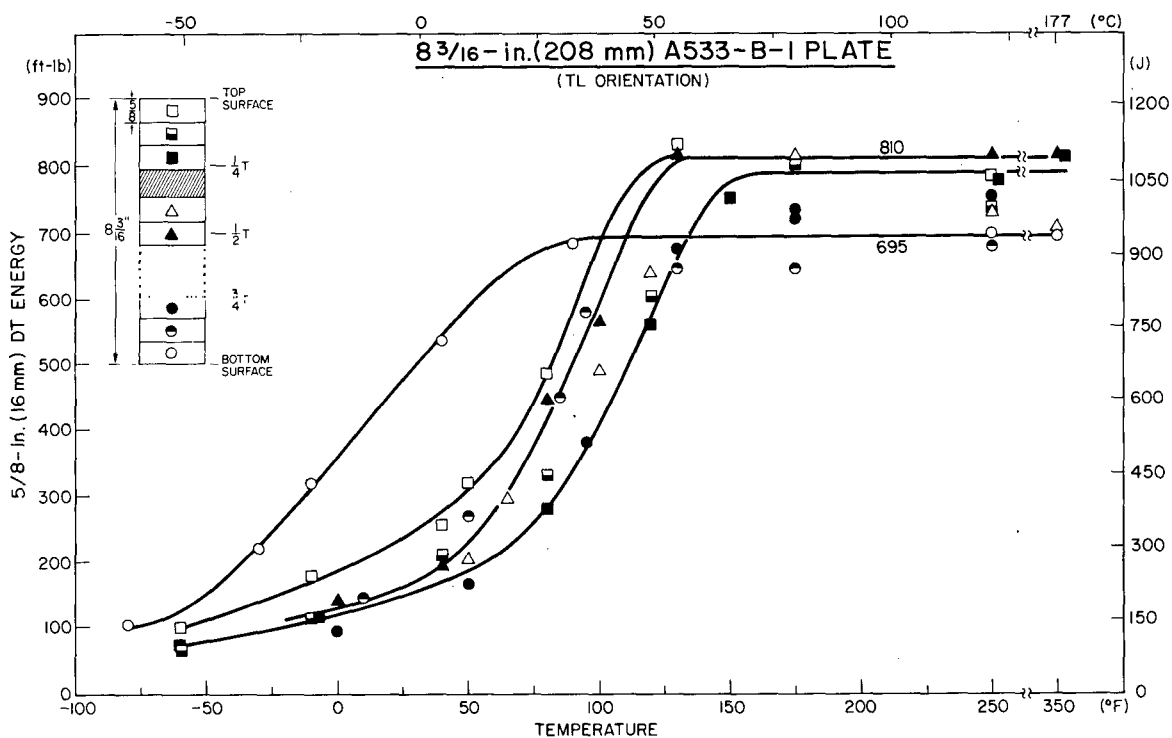


Fig. 13 — Dynamic tear (DT) test performance of the A533-B steel plate at various positions through the plate thickness. The test specimens were 5/8 in. (16 mm) thick and were oriented in the transverse (TL) direction.

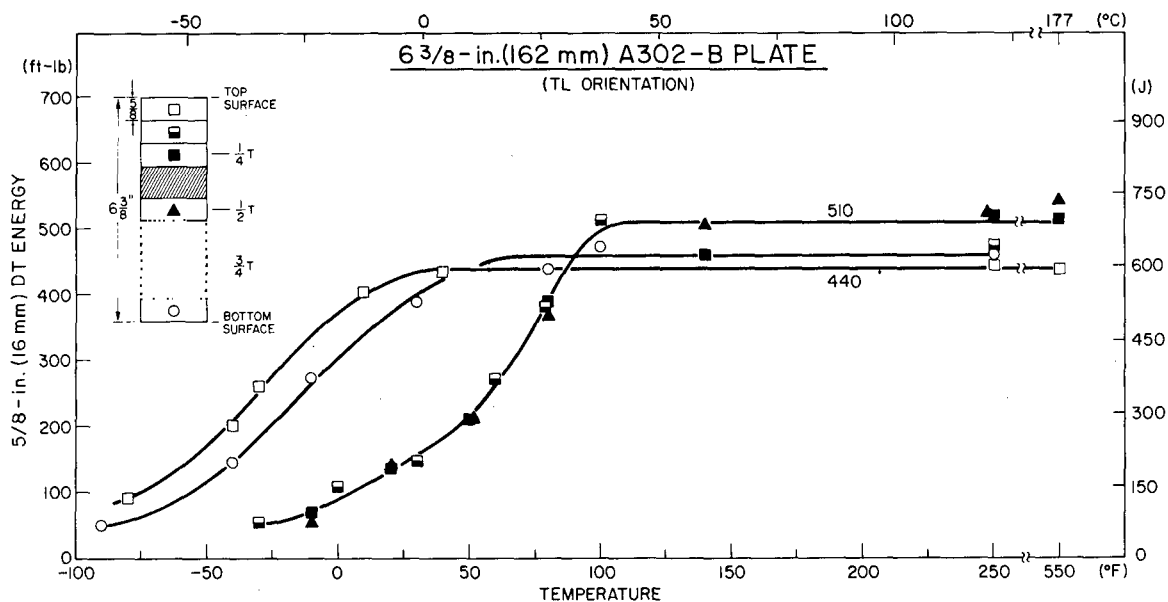


Fig. 14 — Dynamic tear (DT) test performance of the A302-B steel plate at various positions through the plate thickness. The test specimen orientation was transverse (TL).

*K<sub>Id</sub> Experimental Procedure*

**Precracked C<sub>v</sub> (PCC<sub>v</sub>) Tests.** The PCC<sub>v</sub> tests were conducted in accordance with procedures developed under the EPRI program on Fracture Toughness Data for Ferritic Nuclear Pressure Vessel Materials [6]. Specimens were precracked to a nominal ratio of crack depth to width (a/W) of 0.5. The applied *K*-level was 17 ksi√in. (18.7 MPa√m) for the final 0.025 in. (0.6 mm) of precrack. The data were obtained at impact velocities of 66 and 98 in./s (1.7 and 2.5 m/s). The Charpy machine was equipped with a Dynatup system to define the hammer load vs time behavior and was recorded on a Nicolet Model 1090 transient recorder. The system response time was 87.5 μs in accordance with the requirements given in Ref. 6.

The shape of the PCC<sub>v</sub> hammer load vs time record for each specimen was used to categorize the specimens with respect to fracture before or after general yield.\* With fractures before general yield, the maximum load was used in conjunction with the ASTM E-399 [7] equation for *K<sub>Ic</sub>* under static loading. These data could be considered as valid if the ASTM E-399 rules for static testing are determined to be applicable and if the dynamic yield stress is used. The *K* values for fractures after general yield, *K<sub>Id</sub>*, were computed using the energy to maximum load (corrected for machine compliance), *E<sub>I</sub>*, in conjunction with the J-Integral approximate equation for a deeply notched beam in bending [6]:

$$K_{Jd} = \left[ E J_{P \max} \right]^{1/2} = \left[ \frac{2E_I E}{bB} \right]^{1/2}, \quad (1)$$

where *E*, *b*, and *B* are Young's modulus, the unbroken ligament and the specimen thickness, respectively, and *J<sub>Pmax</sub>* is the value of the J-Integral to the point of maximum load.

For specimens that exceeded the general yield load, the dynamic yield strength was also determined from the PCC<sub>v</sub> specimens by the methods specified in Ref. 6.

**1-in. (25-mm) Bend Specimens.** The objective here is to develop a generalized procedure for measurement of *K<sub>Id</sub>* by the use of bend bars having thicknesses of 1 in. and greater. The initial experiments consisted of drop-weight impact tests conducted at various temperatures utilizing specimens 1-in. thick. It is known that the hammer (tup) force vs time behavior during impact loading cannot be employed to compute *K<sub>Id</sub>* without special restrictions on the maximum allowable *K̇* and on the system electronics [5]. For this reason the dynamic bending moment at midspan is measured during impact by means of a strain gage close to the crack tip. It is assumed that the bending moment so determined is proportional to the instantaneous stress intensity factor as computed under static loading (ASTM E-399 equation) [7].

\*The mechanism for categorizing failure as to "before" or "after" general yield is explained in Ref. 6



Bend specimens having height (W) and thickness (B) of 1 and 2 in. (25 and 50 mm), respectively, were cut from the program materials. Specimens were fatigue precracked in three-point bending at room temperature at a maximum stress intensity,  $K_f$  (max), of 22 ksi/in. (24.7 MPa/m). The ratio of final crack length to beam height ( $a/W$ ) was approximately 0.5 with the length of fatigue precrack extending a nominal 0.060 in. (1.5 mm) below the machined notch.

Specimens were instrumented with an  $1/8 \times 1/8$  in. (3 mm  $\times$  3 mm), 120-ohm strain gage near the minimum section as indicated in Fig. 15. Care was taken to assure that the strain gage was not mounted in the plastic zone that occurs near the notch in all metals that exhibit a nominal linear elastic behavior. Prior to impact testing, the specimens were calibrated to establish a relationship between the strain gage output and the load (or bending moment) at midspan. This calibration was determined in static, three-point bending at room temperature with the specimen loaded to an applied  $K_I$  of 12 ksi/in. (13 MPa/m). Over this loading range the load-strain relationship for the gage was essentially linear.

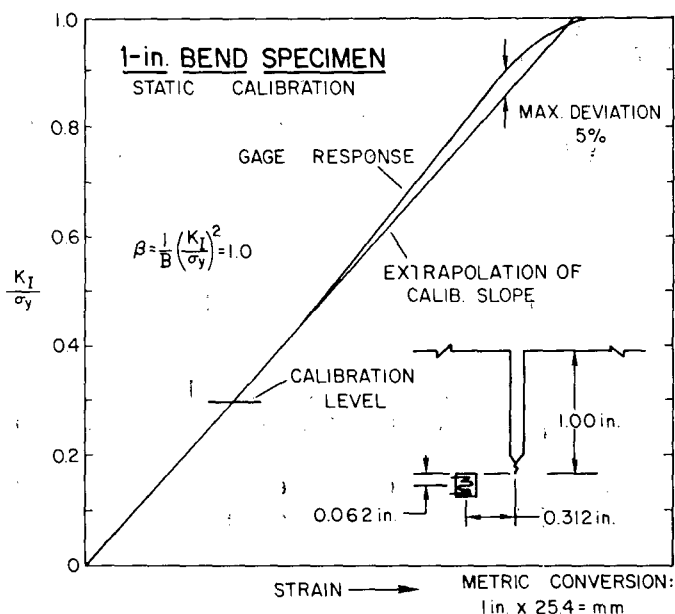


Fig. 15 — Prior to impact, the strain gage is statically calibrated to the level shown. This linear calibration is extrapolated to higher levels of  $K_I/\sigma_y$  so that the gage output during impact loading can be interpreted. An extension of the static calibration to  $K_I/\sigma_y = 1$  shows that the extrapolation error is less than 5 percent, but the data are valid only for  $K_I/\sigma_y \leq 1$  for 1-in. (25-mm) specimens.

During an actual test, the specimen load necessarily exceeds the calibration load. To define the load at fracture, the linear load-strain calibration record was extrapolated to the fracture load (Fig. 15). To validate this extrapolation procedure, several specimens were loaded statically to the loads encountered in the dynamic test. As illustrated in Fig. 15, the load vs strain relationship remains linear (to within 5 percent) up to a value of

$K_I/\sigma_y = 1.0$ . The latter corresponds to  $\beta = 1.0$ , as shown in the figure. For the large-size specimens, the same linear correspondence is expected provided the strain gages and their point of application are scaled geometrically. This scaling has been successfully accomplished for 2-in. (50-mm) thick bend specimens; the resulting load vs strain relationship is also linear up to  $\beta = 1.0$ . Note that if this strain gage technique continues to permit a linear relationship up to a value of  $\beta = 1$ , larger values of  $K_{Id}$  may be determined for the larger specimens. In other words,  $\beta = 1$  for a 1-in. (25-mm) specimen results in  $K_I/\sigma_y = 1.0$  measurement capability, whereas  $\beta = 1$  for a 2-in. specimen corresponds to  $K_I/\sigma_y = 1.4$ .

During a dynamic test the output of the strain gage vs time is monitored on a Nicolet Model 1090 transient recorder. The strain at fracture initiation plus the time of fracture can be assessed from the strain gage output by means of a discontinuity in the trace. Figure 15 is used to translate the strain into terms of equivalent specimen load in three-point bend for the static condition. This procedure has been previously described [5]. It is important to note that this method of assessing the fracture load assumes the correspondence between the bending moment at midspan and the strain gage output to be independent of strain rate. This assumption is felt to be reasonable but is difficult to verify quantitatively in that a two-dimensional analysis of the specimen is required. A one-dimensional analysis of bending moments in the beam is currently underway. From this analysis it is known that a sharp change in bending moment distribution occurs along the length of the beam and that this variation is greater than in the static case. For this reason the strain gage has been placed as close as possible to the notched region to define the bending moment at the section of interest.

The dynamic  $K_{Id}$  is determined from the specimen load at fracture in conjunction with the equation for static  $K_{Ic}$  given in ASTM E-399 [7]. This procedure is similar to that used for the PCC<sub>v</sub> test with one important difference: in the PCC<sub>v</sub> test the hammer load is used, whereas with the bend specimens the load at fracture is taken from the strain gage.

For cases in which the strain gage indicates a value of  $\beta > 1.0$ , the above procedure is not applicable because a linear correspondence between the strain gage and specimen load no longer exists (Fig. 15). Consequently, a J-Integral procedure similar to that used for the PCC<sub>v</sub> specimen (Eq. 1) is used to compute  $K_{Id}$ . In these circumstances, the tup vs time trace must be used to define the energy absorption,  $E_I$ , needed to compute  $J_{Id}$ . Use of the tup load for  $K_{Id}$  is not generally reliable unless special restrictions (i.e., filters) on the system electronics are employed and the fracture time is required to be greater than some minimum value, as has been done with the PCC<sub>v</sub> test [5].

The electronics for the bend specimen currently do not employ filters, and so the J-Integral values may be in error at short times, but should better reflect the true  $J_{Id}$  at larger time periods. This error is related to the oscillations commonly observed in the tup vs time trace. The J-Integral value requires an energy computed through the mean of the tup oscillations. Thus, when the fracture times are short (i.e., 1 to 2 tup oscillations), it is difficult to establish a mean between the tup oscillations; lack of this mean in turn, can result in an error in the computations of  $J_{Id}$ . The use of electronic filters serves to attenuate the tup oscillations to permit an easier definition of the mean behavior.

For the current program, however, filtering is not desirable for two reasons: (a) the use of filters must be coupled with certain minimum times to fracture which would require a reduction in impact velocity and so defeat part of the program objectives, and (b) the unfiltered loads are required to make comparisons with theoretical projections possible.

## Results

A comparison of the 1-in. (25-mm) bend and  $PCC_v$  trends for the program materials is presented in Figs. 16-19. Also illustrated is the  $K_{IR}$  curve from the ASME Code [8]. The latter has been assumed by the Code to represent the lower bound of  $K_{Id}$  vs temperature for the subject class of materials. It is known that the  $K_{Id}$  values for a given material and temperature are a function of the strain rate ( $\dot{K}$ ) to which the material is subjected [9]. In order to facilitate comparisons, the loading rates for the 1-in. bend and  $PCC_v$  specimens were controlled to provide a similar  $\dot{K}$  for both specimens in the range of  $2.1$  to  $2.7 \times 10^5$  ksi/in. s<sup>-1</sup> ( $2.3$  to  $3.0 \times 10^5$  MPa/m s<sup>-1</sup>).\* The  $PCC_v$  specimens were tested in the same manner as in standard  $C_v$  tests (except for the impact velocity). The 1-in. bend specimens were supported on an 8-in. (203-mm) span and loaded by a falling weight from 12 in. (305 mm).

On the basis of the trends in Figs. 16-19, it is concluded that both the  $PCC_v$  and 1-in. (25-mm) bend specimens produce the same value of  $K_{Id}$  in the temperature region below the NDT temperature. This result is expected when both specimens are sufficiently thick to provide plane strain constraint for the low levels of  $K_{Id}$  determined. The agreement of the two results lends support to the adequacy of the strain gage technique that has been developed for the bend specimens. In other words, if a fundamental error existed in the interpretation of the strain gage results, it should have been apparent by a difference between the 1-in. and  $PCC_v$  results in the low temperature regime.

It is important to note a difference in the  $K_{Id}$  trends for the two specimens in the temperature region above the NDT temperature. On balance, the  $PCC_v$  test produces higher  $K_{Id}$  values in this region than does the 1-in. (25-mm) bend specimen. This result is consistent with that observed by Oldfield et al for another heat of A533-B Class 1 steel [10]. On the basis of the present results, a reassessment of the  $PCC_v$  test appears to be required. If the procedure continues to overestimate  $K_{Id}$  in comparison with the 1-in. bend results, then the use of the  $PCC_v$  for initial applications, such as in reactor vessel surveillance, must be justified.

The reason for the difference between the  $PCC_v$  and 1-in. specimen results has not yet been ascertained. The authors suggest the possibility that the  $PCC_v$  specimen, at temperatures above the NDT may undergo a "stable cracking" process. In other words, if the specimen deflection suddenly could have been stopped before maximum load was reached, some crack extension might have been evident. Crack extension of this type would not be permitted in a  $K_{Jd}$  (i.e.,  $J_{Id}$ ) computation. Assessments of stable (rising-load) crack extension using an R-curve approach under static conditions for other materials have indicated large variations (factor of 2) in  $K_{Jd}$  computed on the basis of maximum load vs that computed at the point of crack initiation. When toughness levels are

\* $\dot{K}$  was determined by the ratio of  $K_{Id}$  to the time to fracture.

near 200 ksi  $\sqrt{\text{in.}}$  (220 MPa $\sqrt{\text{m}}$ ), the PCC<sub>v</sub> specimen exhibits a small ductile band at the tip of the fatigue precrack followed by the appearance of a cleavage fracture. This band is believed to have been formed by crack extension prior to the application of the maximum load on the specimen.\* However, in the case of toughness levels below 200 ksi $\sqrt{\text{in.}}$ , the PCC<sub>v</sub> specimens also exhibited toughness levels above those of the 1-in. specimens even though no ductile band was observed at the crack tip. Also, none of the results in Figs. 16-19 for the 1-in. specimen exhibit a ductile region at the tip of the fatigue crack even at toughness levels where this phenomenon is exhibited by the PCC<sub>v</sub> specimen.

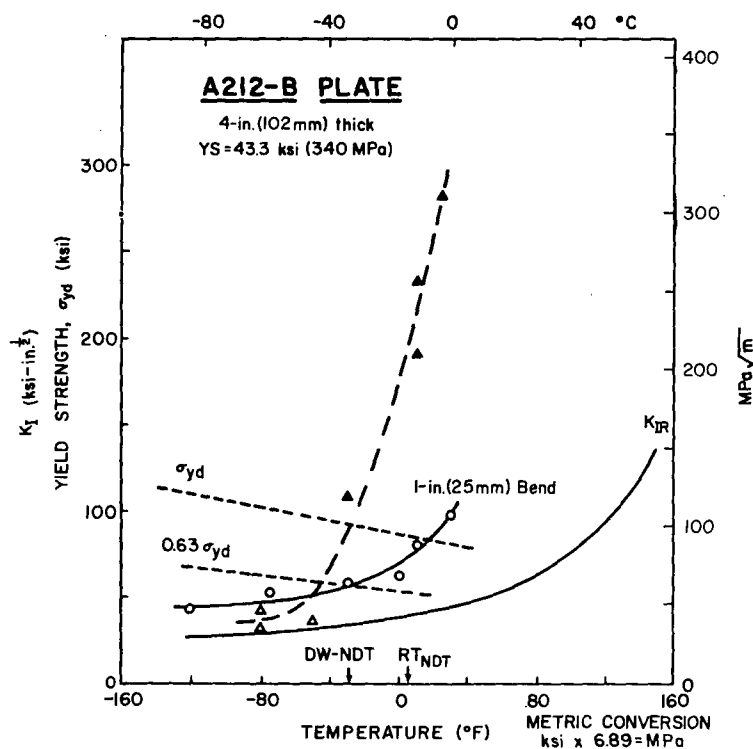


Fig. 16 — Comparison of dynamic fracture toughness trends for the A212-B reference plate. Both 1-in. (25 mm) bend and PCC<sub>v</sub> specimens exhibited a  $\dot{K} \approx 2.5 \times 10^5$  ksi $\sqrt{\text{in.}}$  sec<sup>-1</sup> ( $2.8 \times 10^5$  MPa $\sqrt{m}$  s<sup>-1</sup>). The open symbols represent fracture before general yield; the filled triangles represent points computed by a J-integral procedure. In this procedure specimen energy to the point of maximum load was used in the computation. Both specimens were cut in the LT orientation.

\*The cleavage region is evidenced by a sharp drop in the load vs time record. As long as that load drop corresponds to the maximum load on the test record, it follows that the ductile band must have occurred at loads less than the maximum load which is synonymous with the beginning of the cleavage instability.

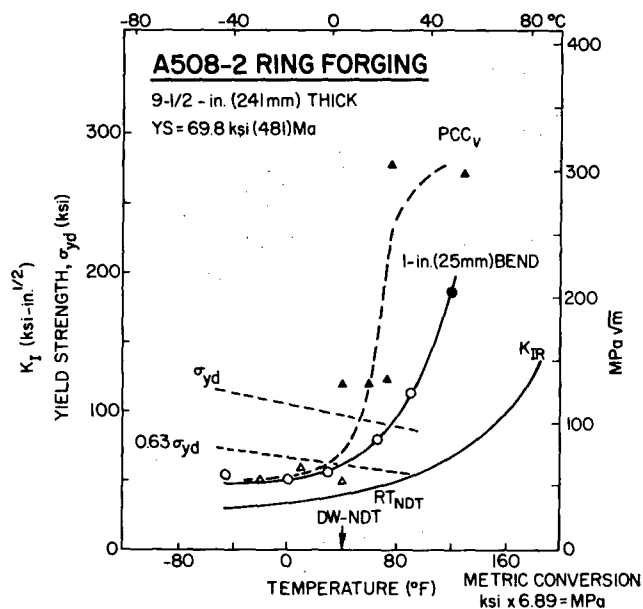


Fig. 17 — Comparison of dynamic fracture toughness trends for an A508 Class 2 forging. Both 1-in. bend and  $PCC_V$  specimens exhibited a  $\dot{K} \approx 2.5 \times 10^5$  ksi/in.sec<sup>-1</sup> ( $2.8 \times 10^5$  MPa/m s<sup>-1</sup>). Both types of specimens were cut in the same orientation and from the same location within the forging. The use of symbols is the same as in Fig. 16.

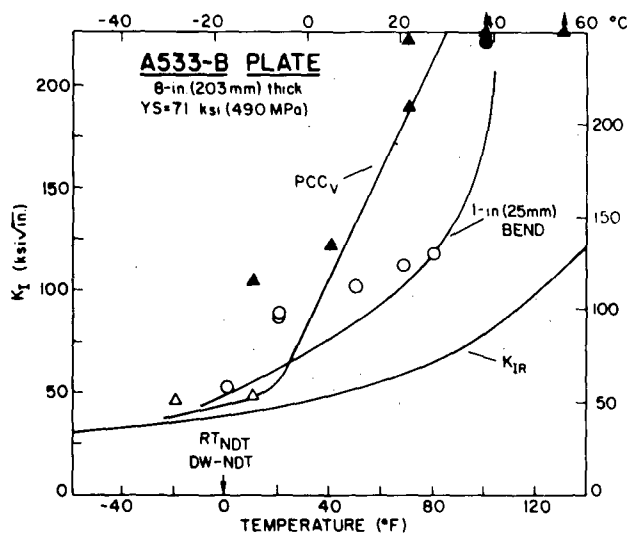


Fig. 18 — Comparison of dynamic fracture toughness trends for an A533-B Class 1 plate. Both 1-in. bend and  $PCC_V$  specimens exhibited a  $\dot{K} \approx 2.5$  to  $3 \times 10^5$  ksi/in.sec<sup>-1</sup> ( $2.8$  to  $3.3 \times 10^5$  MPa/m s<sup>-1</sup>). All specimens were cut in the TL orientation. The use of symbols is the same as in Figs. 16 and 17.

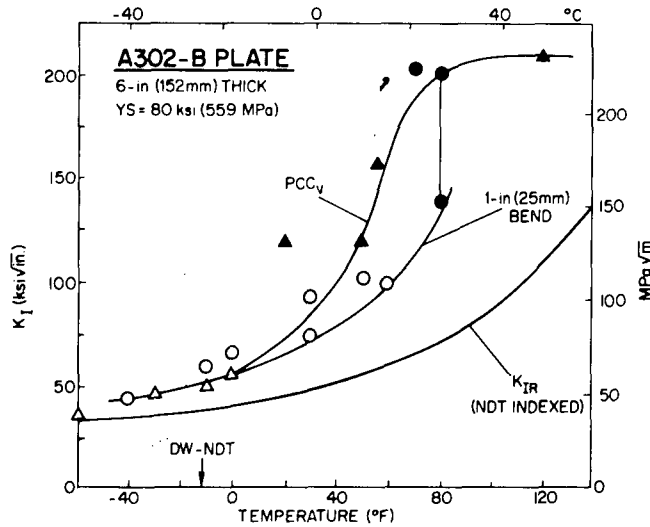


Fig. 19 — Comparison of dynamic fracture toughness trends for an A302-B plate. Both 1-in. bend and PCC<sub>v</sub> specimens exhibited a  $\dot{K} \approx 2.5$  to  $3 \times 10^5$  ksi/in. sec<sup>-1</sup> ( $2.8$  to  $3.3 \times 10^5$  MPa√m s<sup>-1</sup>). All specimens were cut in the TL orientation. The use of symbols is the same as in the three preceding figures.

The results from the 1-in. specimens have highlighted still another phenomenon. Figure 20 presents a generalized plot of the load vs time behavior of the strain gage on the specimens during impact. The circled points represent the fracture initiation for different specimens. In terms of the oscillations defined by the strain gage, no fractures have been observed in regions of the valleys, which are the shaded regions in the figures. This result is not unexpected since there is no apparent reason why the specimen should fail at a lower load (valley) after first having sustained a higher load (peak). Notwithstanding this rationalization, the observed behavior in Fig. 20 leads to an inconsistency between the  $K_{Id}$  values determined: (a) from the fracture load, and (b) from the J-Integral using the area under the load vs time trace to the point of fracture initiation. In the region of linear elastic behavior, the  $K_{Id}$  can be defined directly from the specimen load in conjunction with ASTM E-399 procedures. However, in the region of a valley, this load corresponds to two different specimen energies (i.e., area under the load-time trace) and hence two different  $K_{Id}$  values determined from the J-Integral procedure. Although the discrepancy in  $K_I$  is less than 15 percent (30 percent in J) near a  $K_{Id}/\sigma_{yd}$  ratio of unity, it points out the need to establish restrictions when the J-Integral analysis is applied to a dynamic situation. In a strict sense, the derivation of J-Integral does not address the acceleration phenomenon experienced by a body under impact loading.

## NRL REPORT 8006

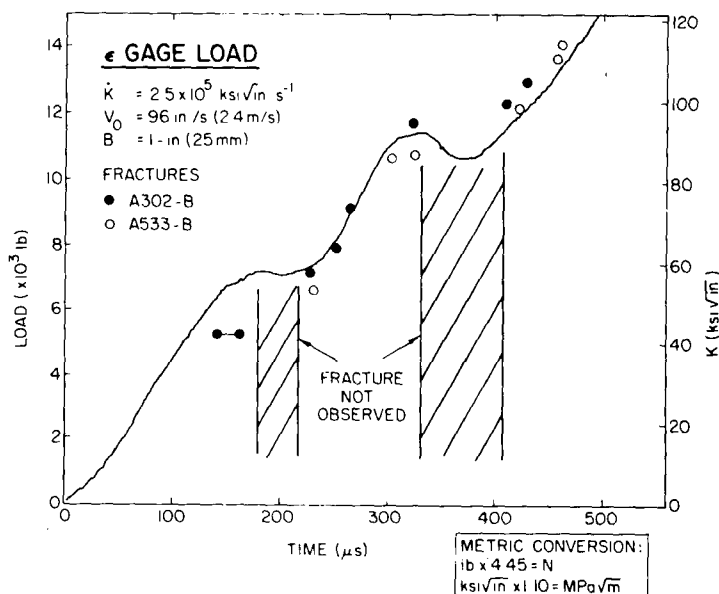


Fig. 20 -- Load vs time behavior exhibited by the strain gage close to the crack tip in 1-in. bend specimens. The fracture times for various specimens are illustrated. The decreasing  $\dot{K}$  in certain regions precludes fracture from taking place in these regions.

## B. Further Analytical and Experimental Study of Inertial Loading in Notched-Beam Impact Tests

C.A. Griffis

### Introduction

To facilitate the experimental measurement of  $K_{Id}$  and to gain greater understanding of the influence of inertial loading in notched-beam impact tests, a dynamic analysis has been undertaken; the goal is to predict the variation in stress intensity factor ( $K_I$ ) with time from the various physical characteristics of the testing system (specimen geometry, impact velocity, and mass and geometry of the striker). The present study is an extension of a previous analytical effort [11] to include the influence of shear deflections, rotary inertia, and higher order bending modes on the response of a notched beam subjected to dynamic, three-point bending. Owing to certain approximations inherent to the one-dimensional analytical model, an extensive experimental assessment of the theory is also in progress.

### Theoretical Development

Assuming that the striker maintains contact with the bend specimen throughout the impact process, the striker velocity,  $\dot{S}(t)$  may be expressed as the sum of the rate of local indentation,  $\dot{\alpha}(t)$ , plus the midspan beam velocity  $v_t(L,t)$ :

$$\dot{S}(t) = \dot{\alpha}(t) + v_t(L, t), \quad (2)$$

where the beam length is  $2L$ . For a drop-weight test characterized by initial velocity,  $V_o$ , a simple application of Newton's 2nd Law to the striker yields:

$$\dot{S}(t) = -\frac{1}{m} \int_0^t F(\tau) d\tau + V_o + gt, \quad (3)$$

where  $m$  is the striker mass and  $F(\tau)$  is the striker force. The rate of indentation at the impact point,  $\alpha(t)$ , is given by:

$$\dot{\alpha}(t) = \frac{d\alpha}{dF} \frac{dF}{dt} \equiv \alpha' \frac{dF}{dt}. \quad (4)$$

In general, the function  $\alpha(F)$  depends upon the striker force, striker geometry, and  $V_o$  [12]. In this work, however,  $\alpha'$  will be regarded as an experimentally determined constant which may be estimated according to Ref. 13:

$$\alpha' \approx V_o / \left( \frac{dF}{dt} \right)_o, \quad (5)$$

where  $(dF/dt)_o$  is the initial slope of the experimentally measured striker force vs time record.

An approximate expression for the midspan beam velocity  $v_t(L, t)$  may be obtained by representing the actual notched beam as two smooth Timoshenko beams connected by a rotary spring, as shown in Fig. 21. The spring sustains no shear force and transmits a bending moment of magnitude  $2\gamma v_x(L, t)$ , where  $v_x(L, t)$  is the beam slope at midspan ( $x = L$ ). The spring stiffness,  $\gamma$ , is chosen such that the static compliance of the notched specimen matches that of the beam-spring model; this condition leads to:

$$\frac{EI}{\gamma} = 2W \left[ 0.4 \left( \frac{W}{2L} \right) (1+\nu) + \left( \frac{4a}{3W} \right) H \left( \frac{a}{W} \right) \right], \quad (6)$$

where:

- $E$  = Young's modulus
- $I$  = moment of inertia of nominal beam section
- $W$  = beam height
- $a$  = notch depth
- $\nu$  = Poisson's ratio,

and the function  $H(a/W)$  is given in Ref. 14.



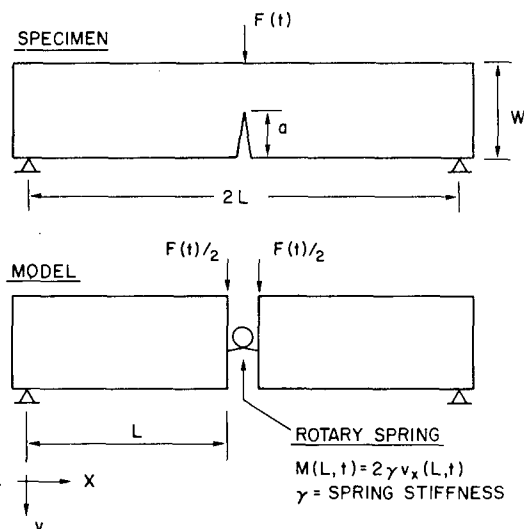


Fig. 21 — Beam-spring idealization of notched bend specimen

Owing to the symmetry considerations, a dynamic analysis of the beam-spring model may be performed by considering only one of the beam segments shown in Fig. 21. Boundary conditions reflect the fact that the beam is simply supported at  $x = 0$  and sustains an applied force  $F(t)/2$  and bending moment  $2\gamma v_x(L, t)$  at  $x = L$ . The well-known stress-displacement relationships for a Timoshenko beam are [15]:

$$M = -EI\Theta_x \quad (7a)$$

$$Q = kAG(v_x - \Theta), \quad (7b)$$

where:

- $M$  = bending moment
- $Q$  = shear force
- $k$  = shape factor for cross section
- $A$  = cross-sectional area
- $G$  = shear modulus.

In Eqs. (7a) and (7b),  $v$  and  $\Theta$  refer to the beam deflection and rotation, respectively. The quantities  $M$ ,  $Q$ ,  $v$ , and  $\Theta$  are understood to be functions of  $x$  and  $t$ . Summation of forces and moments over an elemental length of the beam, leads to two equations of motion [15]:

$$\rho v_{tt} = kG(v_{xx} - \Theta_x) + q(x, t) \quad (8a)$$

$$I\rho\Theta_{tt} = EI\Theta_{xx} + kAG(v_x - \Theta), \quad (8b)$$

where  $q(x,t)$  represents the intensity of the distributed load along the beam length. The boundary conditions referred to above are given by:

$$v(0,t) = 0 \quad (9a)$$

$$\Theta(0,t) = 0 \quad (9b)$$

$$-EI\Theta(L,t) = 2\gamma v_x(L,t) \quad (9c)$$

$$2q(x,t) = F(t)\delta(x - L), \quad (9d)$$

where  $\delta(x - L)$  represents the Dirac-delta function.

Initial conditions for all the problem at hand express the fact that the beam is initially at rest, i.e.,

$$v(x,0) = \Theta(x,0) = v_t(x,0) = \Theta_t(x,0) = 0. \quad (10)$$

The boundary value problem posed by Eq. (8) through (10) may be readily solved using the method of superposition of normal modes [15], whereby the (series) solution obtained for the free vibration case is employed to construct the forced vibration response. Omitting the lengthy mathematical details, the displacement and rotation are given by:

$$v(x,t) = \sum_{i=1}^{\infty} \frac{f_i(x)f_i(L)}{2\rho AH_i\omega_i} \int_0^t F(\tau) \sin[\omega_i(t-\tau)] d\tau \quad (11a)$$

$$\Theta(x,t) = \sum_{i=1}^{\infty} \frac{g_i(x)g_i(L)}{2\rho AH_i\omega_i} \int_0^t F(\tau) \sin[\omega_i(t-\tau)] d\tau. \quad (11b)$$

Explicit mathematical expressions for the modal functions ( $f_i$  and  $g_i$ ), natural frequencies ( $\omega_i$ ), and normalization constant ( $H_i$ ) have been developed and will appear in a forthcoming publication.

Substitution of Eqs. (3) and (4), and the time derivative of Eq. (11a) into Eq. (2) yields the following integral equation:

$$\begin{aligned} -\frac{1}{m} \int_0^t F(\tau) d\tau + V_o + gt = \alpha' \frac{dF(t)}{dt} \\ + \sum_{i=1}^{\infty} \frac{f_i^2(L)}{2\rho AH_i} \int_0^t F(\tau) \cos \omega_i(t-\tau) d\tau. \end{aligned} \quad (12)$$

## NRL REPORT 8006

Solution of Eq. (12) subject to the initial condition,  $F(0) = 0$ , makes possible the prediction of the striker force vs time history. When  $F(t)$  has been obtained, the midspan bending moment is easily computed from Eqs. (11b) and (7a). Finally, an estimate of the time-dependent stress intensity factor can be made if it is assumed that the relationship between  $K_I(t)$  and midspan bending moment,  $M(L, t)$ , is independent of loading rate [13,16]. Thus, from static fracture mechanics:

$$K_I(t) = \frac{6M(L,t)a^{1/2}}{BW^2} Y(a/W), \quad (13)$$

where  $Y(a/W)$  is given in Ref. 17. It must be emphasized that use of Eq. (13) for dynamic loading is open to question and will require further two-dimensional analysis for an assessment of its applicability.

### Results

To examine the nature of the analytical predictions, calculations have been performed for a drop-weight test having parameters indicated in Fig. 22. These test conditions roughly correspond to those existing in previously described tests [5] on pressure vessel steel. In Fig. 22, the computed striker load,  $F(t)$ , has been multiplied by  $L/2$  to represent a "static" bending moment at midspan, i.e., that moment which would exist at the notched section if the specimen were slowly loaded by a force  $F(t)$ . Also indicated in the figure is the computed *dynamic* moment at midspan,  $M(L, t)$ , with the right-hand ordinate giving the projected  $K_I$  values according to Eq. (13). The  $F(t)$  history was computed using numerical, step-by-step integration of Eq. (12) with an integration interval of  $2.5 \mu s$ . Adequate convergence of the solution was observed by including only the first twenty terms of the infinite series appearing in Eq. (12).

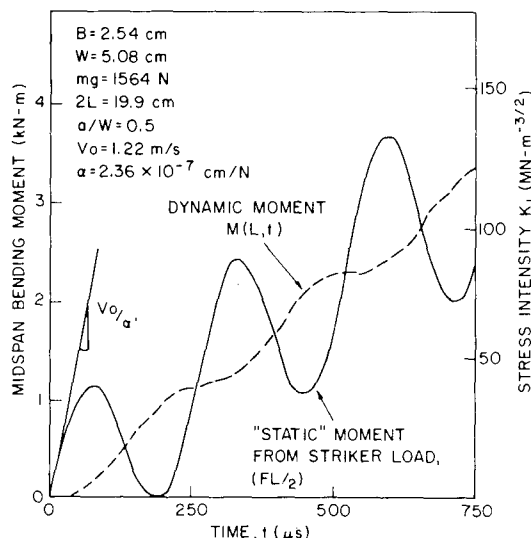


Fig. 22 — "Static" and dynamic midspan bending as computed according to beam-spring model

Figure 22 indicates that the "static" moment,  $F(t)L/2$ , oscillates markedly about the true, dynamic bending moment,  $M(L,t)$ . Obviously, if the former were employed in  $K_{Id}$  computations, intolerable errors would be introduced, particularly for fracture times occurring near the peaks or valleys in the  $F(t)$  history. The present results also imply that the position of maximum load on the  $F(t)$  trace need not correspond to the fracture of the test piece; an oscillatory  $F(t)$  record is expected solely on the basis of mechanical considerations.

### *Further Studies*

To assess the reliability of the analytical model, an experimental test matrix is currently in progress whereby measurements of both the striker force and dynamic bending moment (close to the notched section) are being obtained as functions of time. These measurements will be compared with analytical predictions over a range of impact velocities of  $48 \text{ ips} \leq V_o \leq 192 \text{ ips}$  ( $1.2 \text{ m/s} \leq V_o \leq 4.9 \text{ m/s}$ ) and relative notch depths ( $0.3 \leq a/W \leq 0.7$ ). Standard 1-in. (25-mm) thick bend specimens fabricated from a 5Ni steel ( $YS \sim 145 \text{ ksi}$ ,  $1000 \text{ MPa}$ ) are being utilized in the experimental program. The exceptional toughness ( $K_{Ic} > 175 \text{ ksi}\sqrt{\text{in.}}$ ,  $192 \text{ MPa}\sqrt{\text{m}}$ ) and high yield strength of this material minimize the effects of stable cracking and extensive plasticity. Neither of these characteristics has been considered in the present analysis.

## III. RADIATION SENSITIVITY AND POSTIRRADIATION PROPERTIES RECOVERY

### A. Low Fluence, 550°F (288°C) Radiation Assessment of Nuclear Reactor Vessel Steels Having Variable Copper Content

J.R. Hawthorne and H.E. Watson

#### *Background*

The progressive embrittlement of reactor structural steels with increasing neutron exposure has been shown to be nonlinear with fluence ( $\text{n/cm}^2 > 1 \text{ MeV}$ ) and to be dependent upon the content of copper and phosphorous impurities. The bulk of current information on radiation-induced embrittlement has been developed with the Charpy-V ( $C_v$ ) test method. Through  $C_v$  data compilations and analysis, embrittlement trends are being evolved for guidance of reactor design and fracture-safe operation. One example of the use of radiation embrittlement vs neutron fluence curves is the recently issued Nuclear Regulatory Commission Regulatory Guide 1.99, "Effects of Residual Elements on Predicted Radiation Damage to Reactor Vessel Materials."

Trend curve development efforts, to date, have been impeded by a lack of radiation data for the extremes of the fluence range of service. Projected end-of-life fluences for currently operating reactor vessels are on the order of  $3 \text{ to } 5 \times 10^{19} \text{ n/cm}^2$ . A large

## NRL REPORT 8006

volume of data exists for this fluence interval; however, for exposures below  $1 \times 10^{19}$  n/cm<sup>2</sup> data are scarce. The special importance of the low fluence interval is readily brought into focus by reference to the Code of Federal Regulations (10CFR 50). Its specifications make any reactor vessel materials automatic candidates for in-service surveillance programs whenever projections indicate that a minimum embrittlement level (low) will be exceeded. Requirements on minimum upper shelf toughness and on maximum transition temperature increase are also set forth. If, as has been questioned, Regulatory Guide 1.99 embrittlement projections are overly pessimistic, significant material penalties incurred in some cases may be unwarranted.

The current study explores low fluence radiation resistance for two reactor steel types and assesses experimentally the conservatism in Regulatory Guide 1.99 trend projections.

### *Progress*

The  $C_v$  notch ductilities of two pressure vessel steel plates (A533-B and A302-B) and one submerged arc weld deposit (A533-B) have been assessed after 550° F (288° C) irradiation to  $9.5 \times 10^{17} > 1$  MeV. The materials are fully representative of reactor vessel materials now in service and were selected additionally for their difference in impurity copper content. Copper contents were 0.13%, 0.21%, and 0.36%, respectively. Phosphorous contents were 0.008%, 0.015%, and 0.015%, respectively. To facilitate postirradiation comparisons, the materials were exposed simultaneously using a randomized specimen array.

Figure 23 illustrates both the pre- and postirradiation notch ductility of the weld deposit. The data depict a significant increase in the brittle-ductile transition whether measured at the 50 ft-lb or 30 ft-lb (67.8 or 40.7 J) energy level. The drop-weight nil ductility transition (NDT) temperature of the weld deposit before irradiation was -30° F (-34° C) [18]. For the plate materials, smaller elevations in transition temperature were found. The elevation for the A302-B plate with 0.21% copper was 40° F (21° C) maximum and essentially nil for the A533-B plate with 0.13% copper. Accordingly, the benefit of a low copper content to radiation resistance [19] is shown to begin at a very low fluence.

In contrast to transition temperature response, none of the materials exhibited a degradation in upper shelf energy with low fluence irradiation. The largest radiation effect was shown by the submerged arc weld deposit; however, the upper shelf energy decrease was less than 7% even between the data extremes; i.e., the highest energy value for the unirradiated condition vs the lowest energy value for the irradiated condition.

Good agreement between experimental measurement and Regulatory Guide 1.99 projection was noted for transition temperature behavior with Guide projections slightly conservative for all three materials. In contrast to this comparison, the experimental results indicate that the Guide is overly conservative in predicting upper shelf behavior. For example, in Fig. 24, the measured decrease in upper shelf energy for the weld deposit, was 7% or less, whereas a 30% decrease is the projection for 0.35% copper weld deposits irradiated to a  $9.5 \times 10^{17}$  n/cm<sup>2</sup> fluence. A similar level of conservatism (less than 7% decrease in upper shelf energy) was found when results for the plates were evaluated.

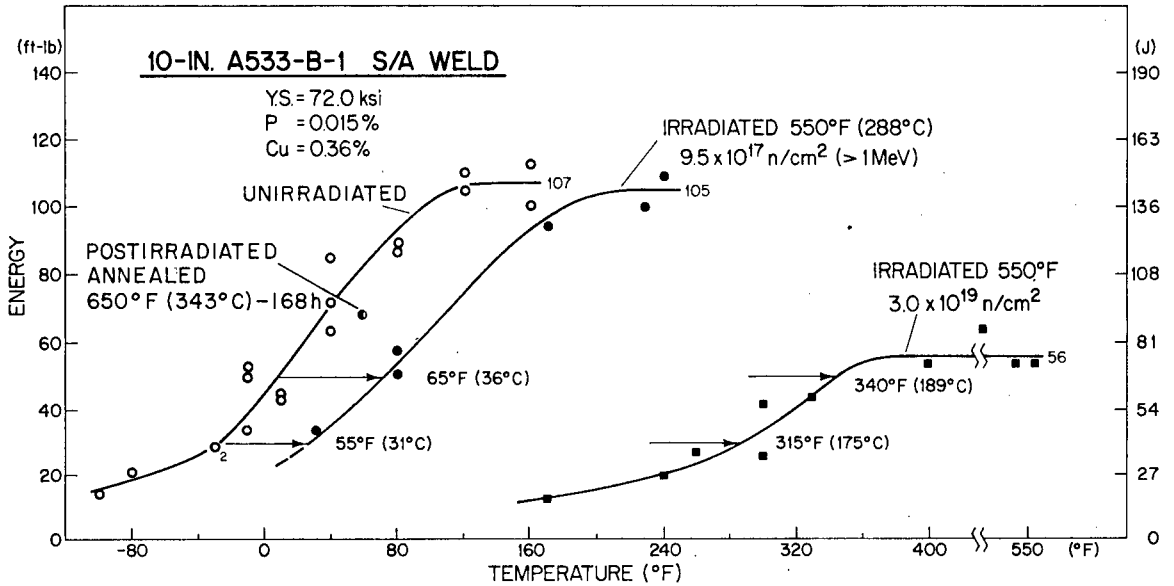


Fig. 23 — Charpy-V notch ductility of the submerged arc weld deposit before and after 550°F (288°C) irradiation. Results for  $3.0 \times 10^{19}$  n/cm<sup>2</sup> irradiation are from an earlier study [18].

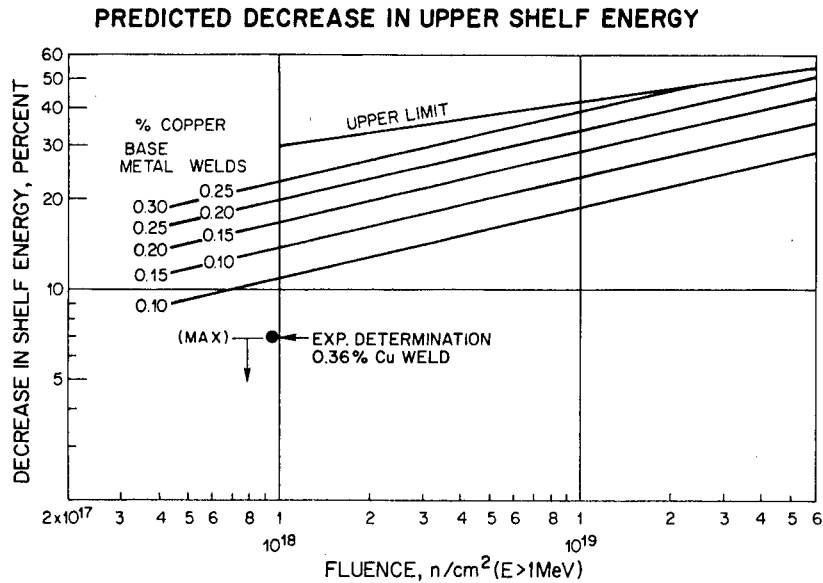


Fig. 24 — Measured upper shelf energy reduction for the submerged arc weld deposit entered on the Regulatory Guide 1.99 graph for projecting postirradiation upper shelf behavior. The upper limit curve applies in this case because of the 0.36% Cu content of the weld.

## NRL REPORT 8006

Although additional verification data are necessary, the findings of this study suggest that the upper shelf is, in fact, quite resistant to low fluence irradiation regardless of copper content and that current upper shelf penalties for low fluence service could be reduced.

**B. Influence of Duplex Metallurgical Microstructure on  
Radiation Embrittlement Resistance of a Reactor  
Pressure Vessel Steel**

J.R. Hawthorne

*Background*

Residual element content presently is well established as a critical variable influencing the resistance of low alloy structural steels to radiation embrittlement [19,21]. A second metallurgical variable suspected of having some influence over elevated temperature radiation resistance is steel microstructure, but experimental confirmation, in this case, was not available.

For reactor pressure vessel steels, the contribution of steel microstructure to elevated temperature (550° F, 288° C) radiation performance is of practical interest. It is noted that microstructures of steels currently used in reactor vessel construction are typically tempered upper bainite. Variations in microstructure, however, do occur with the steels, both between plates and through-the-thickness of individual plates. One variation from the basic structure that is sometimes observed is the presence of proeutectoid ferrite in an upper bainite matrix. Susceptibility to ferrite formation, in general, increases (a) with plate thickness and (b) with decreasing cooling rate from the austenitizing heat treatment.

This study examines, in a closely controlled experiment, the potential effect of a mixed microstructure on 550° F (288° C) radiation resistance for a common reactor pressure vessel steel.

*Progress*

The radiation resistances of three A302-B steel plate sections representing duplex upper bainite and ferrite microstructures or fully upper bainitic microstructures have been compared after irradiation to a fluence of  $4.5 \times 10^{19}$  n/cm<sup>2</sup> at 550° F (288° C). Two of the plate sections were from a 300-lb (136-kg) laboratory melt (Melt 1) featuring a "nominal" residual impurity element content; the third plate section was from a companion laboratory melt (Melt 2) depicting a "low" impurity element content. Plate compositions and the heat treatment schedules used to produce the two microstructural types are given in Table 3. Individual microstructures are documented in Fig. 25. Note that the proportion of proeutectoid ferrite present in each of the duplex microstructures was accentuated metallurgically and represents an extreme case. For direct comparisons of irradiation response, specimens of all three plate sections were irradiated simultaneously in a single reactor experiment.

Table 3  
Chemical Composition and Heat Treatment of A302-B Steel  
Plate Sections

Melt	Normal Residuals		Low Residuals	
Plate Section	1	2	1	
Heat Treatment	A*	B†	A*	
Chemical Analysis (wt.-%)	NRL	U.S. Steel	NRL	U.S. Steel
C	0.24	0.24	0.25	0.28
Mn	1.30	1.37	1.29	1.32
P	0.006	0.014	0.001	0.004
S	0.018	0.019	0.004	0.004
Si	0.28	0.29	0.30	0.33
Ni	0.24	0.18	0.06	0.036
Cr	0.18	0.18	0.08	0.053
Mo	0.55	0.53	0.55	0.52
Cu	0.14	0.19	0.03	<0.005
Ti	0.02	0.017	≤0.01	<0.005
Sn	0.03	0.028	<0.01	0.005
Al	0.02	0.045	0.02	0.041
N	—	0.007	—	0.004

\*Heat Treatment A (duplex microstructure): Austenitized 1 h at 1650°F (899°C); furnace cooled to 1200°F (649°C); held at 1200°F 3 h; furnace cooled to 600°F (316°C); air cooled from this temperature.

†Heat Treatment B: Austenitized 1 h at 1650°F; air cooled; tempered 1 h at 1200°F; water quenched; stress relief annealed by 6 cycles at 1125°F (607°C) for 30 h total.



## NRL REPORT 8006

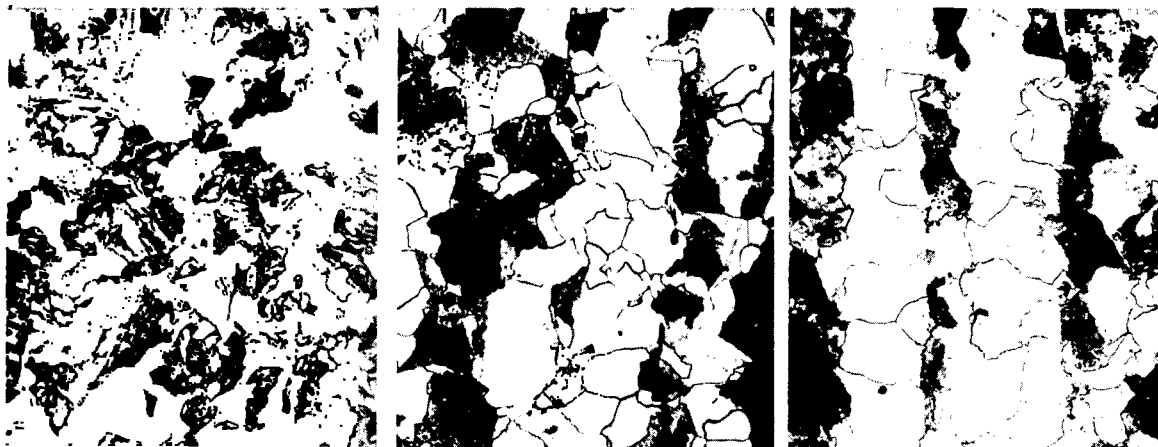


Fig. 25 — Microstructures of the A302-B steel plate sections (500X): (Left) Plate Section 2, Melt 1 (nominal residuals); (Middle) Plate Section 1, Melt 1 (nominal residuals) duplex microstructure of upper bainite and proeutectoid ferrite; and (Right) Plate Section 1, Melt 2 (low residuals) duplex microstructure of upper bainite and proeutectoid ferrite

Postirradiation  $C_v$  notch ductility observations for the individual materials are indicated in Figs. 26 and 27. The marked difference in radiation resistance between Melts 1 and 2 for the same microstructural condition was expected and is consistent with the aforementioned detrimental effect of a high residual element content on irradiation performance. Low temperature ( $<300^\circ\text{F}$ ,  $<149^\circ\text{C}$ ) irradiation results, developed earlier, are also included in both figures. In the case of plate section 2 of Melt 1, a variation in notch toughness was observed between the plate sampling locations used for the  $550^\circ\text{F}$  ( $288^\circ\text{C}$ ) irradiation experiment and the  $<300^\circ\text{F}$  ( $<149^\circ\text{C}$ ) irradiation experiment. Accordingly, two curves are shown for the preirradiation condition.

Figure 26 shows that the duplex microstructural condition of Melt 1 is as sensitive to  $550^\circ\text{F}$  ( $288^\circ\text{C}$ ) radiation as the single microstructural condition is; that is, the transition temperature increases with irradiation were about equal at  $170^\circ\text{F}$  ( $94^\circ\text{C}$ ) and  $150^\circ\text{F}$  ( $83^\circ\text{C}$ ), respectively. The results demonstrate that, for the normal residuals case with elevated temperature radiation service, the development of a duplex upper bainite and proeutectoid ferrite microstructure is not particularly detrimental to vessel radiation embrittlement resistance compared to a steel having a fully upper bainite microstructure. From the data given for low temperature irradiation of Melt 1, some adverse effect of a duplex microstructure is also indicated; however, the difference in transition temperature increase again is only 10 to 15 percent.

From Fig. 27 a different determination is made for the case of a low residuals composition (Melt 2). As noted, the  $550^\circ\text{F}$  ( $288^\circ\text{C}$ ) radiation exposure produced some embrittlement of the duplex microstructure. In contrast, earlier tests of the fully bainitic condition [19] indicated no apparent embrittlement after a comparable fluence ( $3 \times 10^{19} \text{ n/cm}^2 > 1 \text{ MeV}$ ) at the same temperature. A duplex microstructure thus would appear to have a detrimental effect on  $550^\circ\text{F}$  ( $288^\circ\text{C}$ ) radiation resistance for a "low" residuals composition only and not for a "nominal" residuals composition.

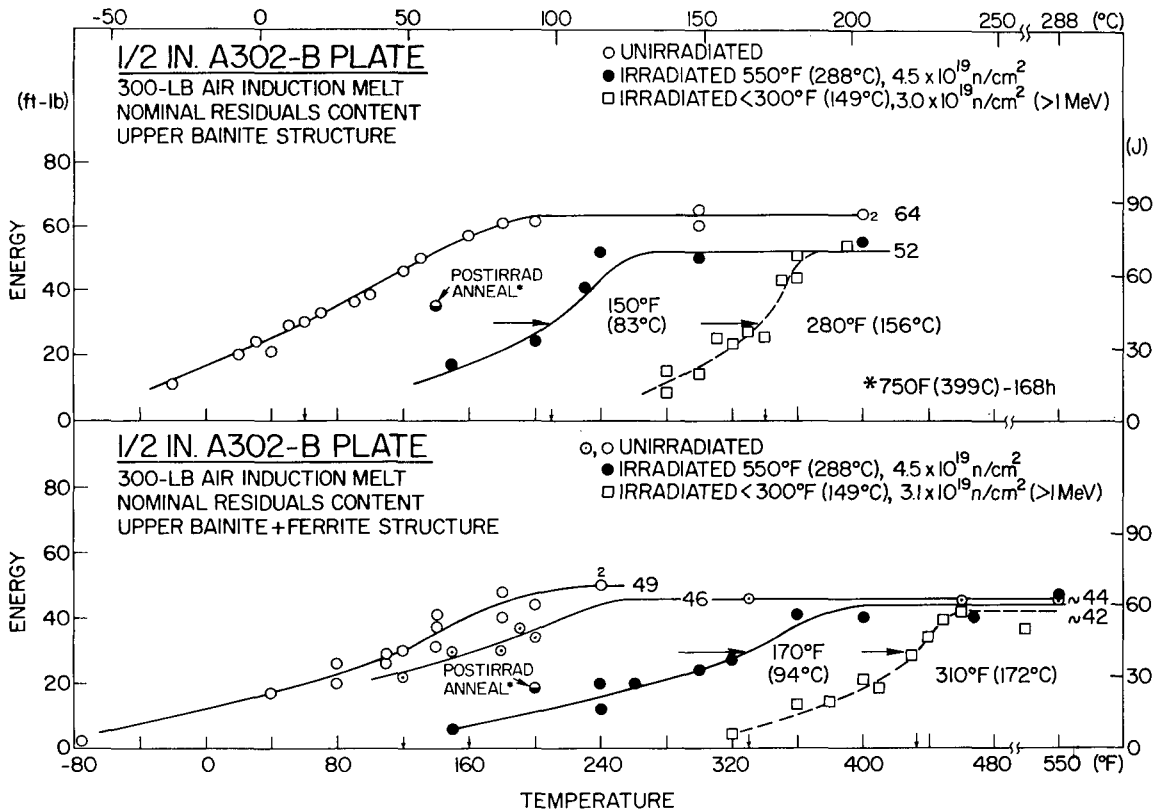


Fig. 26 — Charpy-V notch ductility of plate sections 1 and 2 from laboratory melt 1 containing a nominal residual element content. Residual element content was matched to the ASTM A302-B reference plate employed in reactor pressure vessel surveillance programs. (see Table A2)

## NRL REPORT 8006

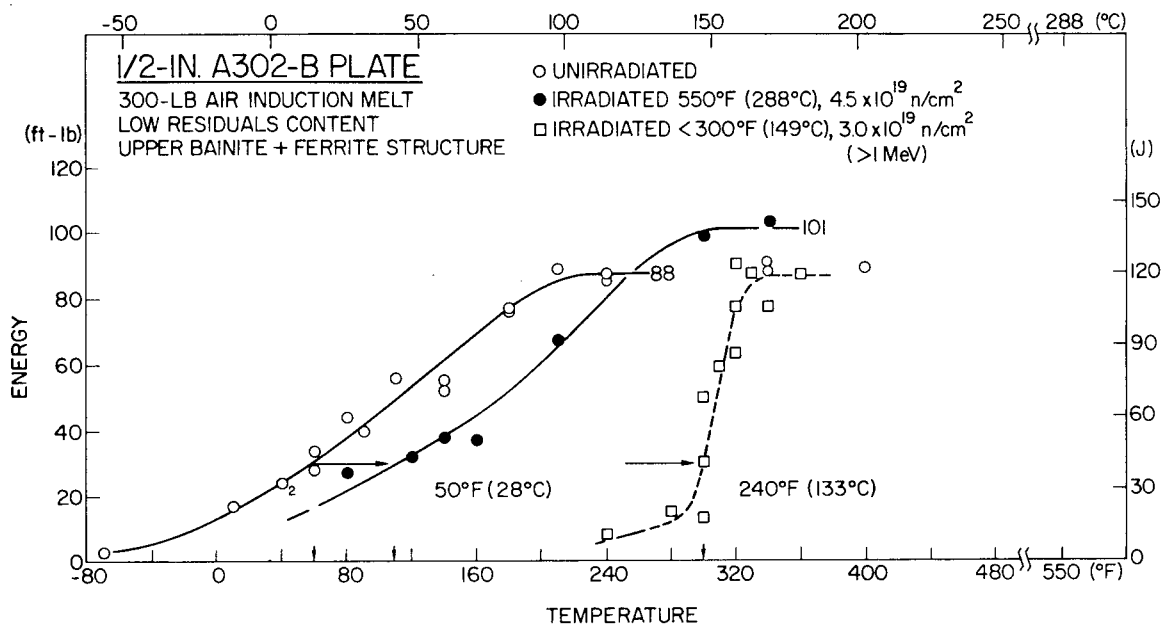


Fig. 27 — Charpy-V notch ductility of a plate section from laboratory melt 2 containing a low residual content. A benefit of a low residual element content to 550°F (288°C) and <300°F (<149°C) radiation resistance is obvious from a comparison of Fig. 27 vs Fig. 26 (lower graph).

Finally, one specimen from each plate section of Melt 1 was investigated to explore the potential influence of microstructure on postirradiation annealing response. The data imply that the duplex microstructure is less responsive to postirradiation heat treatment. The difference in transition temperature recovery denoted in Fig. 26 is considered reinforced by the difference in initial embrittlement levels for the two microstructures.

To complete the present study, instantaneous specimen load vs time records developed using Dynatup test instrumentation will be analyzed for differences in specimen fracture initiation energy and fracture propagation energy. The analyses should be completed for the next quarterly report.

#### IV. THERMAL SHOCK-RELATED INVESTIGATION

##### A. Initial Program Plan for Studies of Warm Prestress and Plastic Net Ligament Phenomena

F.J. Loss and J.R. Hawthorne

##### Background

An experimental program in thermal shock is being conducted by Oak Ridge National Laboratory (ORNL) to evolve a predictive capability for the extension or nonextension of

pre-existing flaws in model vessels. These vessels are subjected to temperatures and applied  $K$ -levels that approximate the conditions in a nuclear pressure vessel when a loss of cooling accident (LOCA) is followed by operation of the emergency core cooling system. During thermal shock, the metal at the crack tip may be influenced by the phenomena of warm prestress and plastic net ligament. NRL will investigate these phenomena and provide information to augment the NRC thermal shock program. Specifically, these studies will:

- Demonstrate the effect of warm prestressing for enhancing the fracture toughness of A533-B steel when flawed material is subjected to a load and temperature history similar to that of the vessel wall during thermal shock.
- Investigate crack propagation and arrest under conditions of limited displacement resulting in a plastic net ligament which simulates the behavior of a deep, longitudinal crack in a vessel during thermal shock.

#### *Warm Prestress Phenomenon*

During thermal shock the applied  $K_I$ -level at a pre-existing flaw attains a maximum early in the LOCA transient (Fig. 28). However, the applied  $K_I$  may not reach the critical ( $K_{Ic}$ ) level until the loading has decreased from the maximum load. The reason is that both  $K_I$  (after the initial maximum) and  $K_{Ic}$  at a given thickness location decrease with time. This "warm prestressing" may preclude failure when  $K_I = K_{Ic}$  unless the applied  $K$ -level exceeds the maximum value that was applied earlier in time. Current thermal shock experiments at ORNL do not incorporate this phenomenon with the small (21-in., 533-mm, o.d.) vessels employed. Consequently, it is necessary to quantify the effects of warm prestressing for the planning and interpretation of future experiments.

#### *Plastic Net Ligament Phenomenon*

As a separate phenomenon during thermal shock, a deep axial flaw can result in a plastic net ligament being formed in the remaining wall thickness (i.e., the vessel will tend to "cusp" as illustrated in Fig. 29. The bend angle ( $\theta$ ) at this location is limited and can be predicted from the known thermal loading. It is projected that crack propagation will arrest due to: (a) the limited bend angle, and (b) the crack propagation into tougher material nearer to the outside wall. To verify this projection it is necessary to develop experimental data.

#### *Approach*

The warm prestressing effect can be demonstrated in a straightforward manner through the use of three-point bend specimens as follows:

1. Load a precracked specimen to the same maximum  $K$ -level attained during thermal shock (at the same relative temperature as the vessel in terms of  $T-RT_{NDT}$ ) (Fig. 28).

## NRL REPORT 8006

2. Slowly decrease both temperature and load to simulate the load-temperature path of the material at the crack tip in a vessel. However, the time scale is not duplicated.

3. If no failure occurs at the temperature and load when  $K_I = K_{Ic}$ , the margin of safety can be demonstrated as follows (see Fig. 28):

a. Maintain the above temperature and increase the load to failure.

b. Maintain the above load and decrease the temperature so that  $K_I/K_{Ic}$  becomes substantially greater than unity. If no failure occurs at this point, the load is increased to failure.

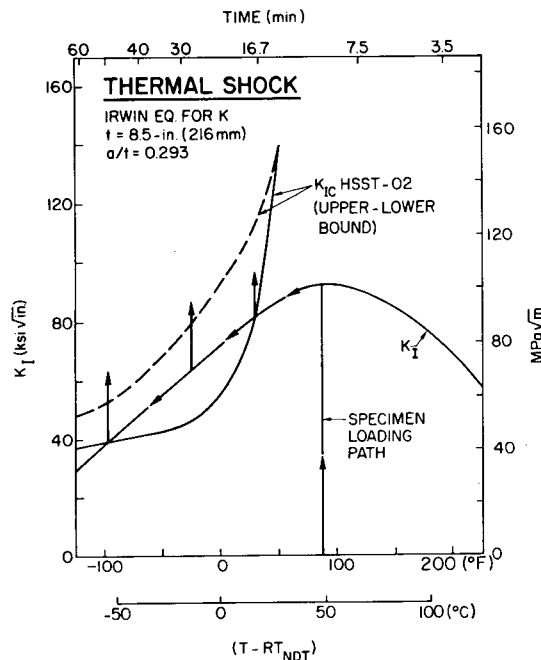


Fig. 28 — Representation of the  $K$ -levels experienced by the material at the tip of a flaw in prototype nuclear vessel (thickness  $t$  and crack depth to thickness  $a/t$  as shown) undergoing thermal shock. The measured  $K_{Ic}$  trends of the specimen material are also shown. These specimens will be loaded as illustrated to define the warm prestress phenomenon. The time scale originates at the instant of the pipe rupture;  $RT_{NDT}$  refers to the reference temperature as defined in Section III of the ASME Boiler and Pressure Vessel Code [8].

## PLASTIC NET LIGAMENT—VESSEL

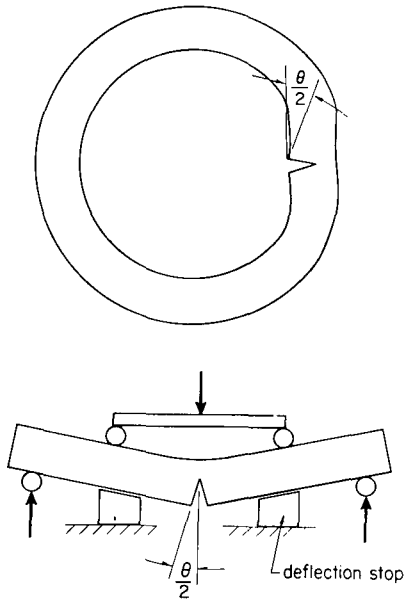


Fig. 29 — Representation of the “cusp” which is formed by a vessel that contains a deep axial flaw and is subjected to thermal shock. The bend angle ( $\theta$ ) at the flaw tip is limited by the imposed thermal loading and will be simulated in the laboratory using four-point bend specimens.

The crack behavior in the case of a plastic net ligament likewise may be determined by investigating bend specimens. In this case four-point bend specimens are preferred since their use will result in a case of pure bending for the test material, which better approximates the thermally-induced bending in an actual vessel. Specimens are loaded so as not to exceed the final bending angle predicted for the cracked vessel. The temperature is held constant during the test.\* More sophisticated, follow-on, experiments may be considered for subjecting the specimen to a linear temperature distribution corresponding to that actually existing in the uncracked ligament during thermal shock.

### Experimental Investigation

**1. Test Material.** Limited material for the program has been obtained from ORNL in the form of 12-in. (305mm) A533-B Class 1 plate (HSST plate 02). This material was chosen because its static  $K_{Ic}$  behavior already has been well characterized in thick sections [9]. This plate has been sectioned to provide specimens within the range of uniform toughness between the 1/4 T and 3/4 T planes.

**2. Specimens.** Fatigue precracked specimens of ASTM E399 proportions ( $a/W = 0.4$ ) have been prepared in two thicknesses (1.5 and 3 in., 38 and 76 mm) in order to investigate the significance of thickness-constraint with respect to warm prestressing and plastic net ligament phenomena. The  $K_{max}$ -levels incurred during fatigue precracking were generally limited to 20 ksi  $\sqrt{\text{in.}}$  (22 MPa $\sqrt{\text{m}}$ ) and 25 ksi $\sqrt{\text{in.}}$  (27 MPa $\sqrt{\text{m}}$ ) for the 1.5-in. and 3.0-in. specimens, respectively. Approximately forty-eight (48) 1.5-in. and fourteen (14) 3-in.

\*It is assumed that the actual temperature distribution will lie within the fully ductile (upper shelf) regime. Hence, the metal toughness is essentially independent of temperature.

## NRL REPORT 8006

specimens are being machined. A portion of each specimen will be side grooved, 5 percent on each side, in an attempt to maintain fatigue crack front straightness so as to represent a portion of a long crack in a vessel.

**3. Analytical Basis.** Plastic net ligament experiments must be based on a knowledge of the rotation of the vessel wall containing a deep flaw. (This rotation results in a cusp in the vessel wall, Fig. 29.) A theoretical estimate of this rotation for a given notch depth has been prepared by G.R. Irwin (University of Maryland). Likewise, the applied  $K_I$ -level must be known as a function of time (or temperature) for a given size flaw. A theoretical determination of this  $K_I$ -level (similar to Fig. 28) has been prepared by E.K. Lynn (NRC) using the Irwin equation for the flawed vessel wall with dimensions and thermal shock conditions that represent those expected in a typical pressurized water reactor plant.

For the vessel geometry illustrated in Fig. 29, Irwin [22] computed the maximum bend angle ( $\theta_{\max}$ ) that would be applied during the thermal loading of a deeply notched vessel as:

$$\theta_{\max} = \frac{2K_{Ic}^2}{E\sigma_{ys}b}, \quad (14)$$

where  $E$  is Young's modulus,  $b$  is the width of the uncracked ligament and  $K_{Ic}$  is the toughness of the material. If one assumes that the toughness,  $K_{Ic}$ , is equal to 200 ksi√in.\* (220 MPa√m) and that the unbroken ligament is 1.0 in. (25 mm), then the maximum bend angle is approximately 2 degrees. A demonstration test imposing a 2-degree bend angle without evidence of crack extension will quantify the inability of the material to sustain crack extension under thermal shock.

**4. Test Matrix.** The first warm prestress bend tests are currently being loaded to the (relative) temperature and  $K$ -profile that is illustrated in Fig. 28. The test specimen has the following geometry:

Vessel wall	=	8.5 in. (216 mm)
$a/t$	=	0.293
Peak applied $K_I$	=	94 ksi√in. (103 MPa√m)

Other specimens will be subjected to conditions resulting from different flaw depths ( $a/t$ ). Because of the limited specimen thickness, care must be taken to insure that the plastic zone† developed in the bend specimen does not exceed that in the thicker vessel wall (having greater mechanical constraint) at the same applied  $K$ -level. Consequently, it may not be possible, in all cases, to apply the peak level of  $K$  that was predicted on the basis of the analysis of Fig. 28. The former will be accomplished by limiting the maximum applied  $K$  for a given size specimen to levels within the range covered by the rules of

\*The trend of  $K_{Ic}$  vs temperature in Fig. 29 leads one to conclude that the  $K_{Ic}$  of the material is in excess of 200 ksi√in. (220 MPa√m) for a metal temperature that is assumed to be in excess of 200°F (93°C).

†The plastic zone radius,  $r_p$ , is formally computed in plane strain as follows:  $r_p = 1/(6\pi) (K_I/\sigma_{ys})^2$ , where  $\sigma_{ys}$  is the yield stress at the test temperature.

ASTM E-399. For a yield strength of 70 ksi (483 MPa), the maximum  $K$ -levels permitted by E-399 are 77 and 54 ksi $\sqrt{\text{in.}}$  (85 and 59 MPa $\sqrt{\text{m}}$ ) for the 3-in. and 1.5-in. (76mm and 38mm) specimens, respectively. With respect to Fig. 28, this restriction will be incorporated by truncating the loading path at the  $K$ -levels required for the given thickness specimen but otherwise proceeding with the indicated loading sequence.

The results of the warm prestressing experiments are complicated by the observed scatter in  $K_{Ic}$  properties for this material [9]. The  $K_{Ic}$  curves in the figure represent the upper and lower bound of valid ASTM  $K_{Ic}$  values obtained for this plate. Because of the scatterband, one cannot *a priori* define the  $K_{Ic}$  at a given temperature. Hence, the intersection of the  $K$  and  $K_{Ic}$  curves may not result in crack initiation (in the absence of a warm prestressing effect) if, in fact, the particular material of the test specimen exhibits a  $K_{Ic}$  as defined by the upper boundary of the scatterband. To resolve this issue the authors are investigating a statistically designed test matrix. However, a positive demonstration of the warm prestress effect can still be defined by lowering the final test temperature sufficiently (i.e.,  $T - RT_{NDT} = 100^\circ\text{F}$  ( $38^\circ\text{C}$ ) in Fig. 28) such that the upper limit of the  $K_{Ic}$  scatterband lies below the maximum applied  $K$ -level.

The phenomenon of plastic net ligament will occur only for a deep crack. Since the uncracked ligament is relatively distant from the cooling water, the metal temperature is expected to remain above  $200^\circ\text{F}$  ( $93^\circ\text{C}$ ) for the time interval of interest. Previous research has shown that at this temperature this plate material lies in the ductile regime and is incapable of brittle behavior. Consequently, a plastic net ligament experiment at this temperature is not expected to produce unstable fracture. However, a demonstration test will be conducted to verify the prediction.

Other plastic net ligament studies will be conducted at lower temperatures in the transition region ( $0$ - $200^\circ\text{F}$ ,  $-18$  to  $93^\circ\text{C}$ ), where the metal can exhibit a brittle fracture mode. Initial tests will be conducted isothermally at a temperature which results in crack initiation prior to reaching the permitted specimen deflection. An arrest behavior under these conditions should provide a positive demonstration of the inability of the crack to penetrate the vessel wall under the limited wall rotation dictated by the thermal shock conditions. Later this test procedure may be augmented to produce a linear temperature distribution through the specimen that more closely approximates the conditions in the vessel. However, *a priori* demonstration of arrest behavior under isothermal conditions at a conservatively low temperature may obviate the need for this later experimental phase.

## REFERENCES

1. W.G. Clark, Jr., and S.J. Hudak, Jr., "Variability in Fatigue Crack Growth Rate Testing," Scientific Paper No. 74-1E7-MSLRA-P2, Westinghouse Research Laboratories, Pittsburgh, Pa., Sept. 18, 1974.
2. ASME Boiler and Pressure Vessel Code, Section XI, Appendix A-4000, Figure A-4300-1, 1974 Edition, ASME, New York, July 1, 1974.



## NRL REPORT 8006

3. T.R. Mager, J.D. Landes, D.M. Moon, and V.J. McLaughlin, "The Effect of Low Frequencies on the Fatigue Crack Growth Characteristics of A533 Grade B Class 1 Plate in an Environment of High-Temperature Primary Grade Nuclear Reactor Water," HSST Technical Report No. 35, Westinghouse Nuclear Energy Systems, Pittsburgh, Pa., Dec. 1973.
4. T.L. Gerber, J.D. Heald, and E. Kiss, "Fatigue Crack Growth in SA508-CL2 Steel in a High Temperature, High Purity Water Environment," ASME, J. Eng. Mat. Tech., **96**, Series H, #4, 1974.
5. F.J. Loss, J.R. Hawthorne, and C.A. Griffis, "Fracture Toughness of Light-Water Reactor Pressure Vessel Materials, Progress Report Ending 28 Feb. 1975," NRL Memorandum Report 3036, Naval Research Laboratory, Apr. 1975.
6. D.R. Ireland and W.L. Server, "Fracture Toughness for Ferritic Nuclear Pressure Vessel Materials, Task A, Program Office Testing and Data Analysis Procedures," ETI Technical Report 74-32, Effects Technology, Inc., Santa Barbara, Calif., May 17, 1974.
7. "Standard Method of Test for Plane-Strain Fracture Toughness of Metallic Materials, E399-74," Book of ASTM Standards, Part 10, ASTM, Philadelphia, Pa., 1975.
8. ASME Boiler and Pressure Vessel Code, Section III, Nuclear Power Plant Components, Subsection NA, General Requirements, 1974 Edition, ASME, New York, July 1, 1974.
9. W.O. Shabbits, "Dynamic Fracture Toughness Properties of Heavy Section A533 Grade B Class 1 Steel Plate," WCAP-7623, Heavy Section Steel Technology Program, Technical Report No. 13, Westinghouse Research and Development Center, Pittsburgh, Pa., Dec. 1970.
10. W. Oldfield, R.A. Wullaert, W.L. Server, and T.R. Wilshaw, "Fracture Toughness Data for Ferritic Nuclear Pressure Vessel Materials, Task A, Program Office, Control Material Round Robin Program," ETI Technical Report 75-34R, Effects Technology, Inc., Santa Barbara, Calif., July 1, 1975.
11. G.E. Nash, "An Analysis of the Forces and Bending Moments Generated During the NRL Dynamic Tear Test," NRL Report 6864, Naval Research Laboratory, Jan. 1969.
12. F.J. Loss, J.R. Hawthorne, and C.A. Griffis, "Fracture Toughness of Light-Water Reactor Pressure-Vessel Materials, Quarterly Progress Report Ending 31 Oct 1974," NRL Memorandum Report 2972, Naval Research Laboratory, Jan. 1975.
13. C.E. Turner, L.E. Culver, J.C. Radon, and P. Kennish, "An Analysis of the Notched Bar Impact Test with Special Reference to the Determination of Dynamic Fracture Toughness," Proceedings, Conference on Practical Application of Fracture Mechanics to Pressure Vessel Technology, London, May 3-5, 1971.

14. J.R. Rice, P.C. Paris, and J.G. Merkle, "Some Further Results of J-Integral Analysis and Estimates," ASTM STP 536, ASTM, Philadelphia, Pa., 1961.
15. Y. Chen, *Vibrations: Theoretical Methods*, Addison-Wesley Publ. Co., Reading, Mass., 1966.
16. G.E. Nash and E.A. Lange, "Mechanical Aspects of the Dynamic Tear Test," Trans. ASME, J. Basic Eng., 91, Series D, 1969.
17. *Plane Strain Crack Toughness Testing of High Strength Metallic Materials*, ASTM STP 410, ASTM, Philadelphia, Pa., 1966.
18. J.R. Hawthorne, J.J. Koziol, and S.T. Byrne, "Evaluation of Commercial Production A533-B Plates and Weld Deposits Tailored for Improved Radiation Embrittlement Resistance," ASTM STP 570, Symposium on Radiation Effects on Structural Materials, Gatlinburg, Tenn. June 11-13, 1974, publ. 1975.
19. U. Potapovs and J.R. Hawthorne, "The Effect of Residual Elements on 550° F Irradiation Response of Selected Pressure Vessel Steels and Weldments," NRL Report 6803, Naval Research Laboratory, Nov. 22, 1968; Nuclear Applications, Vol. 6, No. 1, Jan. 1969.
20. J.R. Hawthorne, "Demonstration of Improved Radiation Embrittlement Resistance of A533-B Steel Through Control of Selected Residual Elements," NRL Report 7121, Naval Research Laboratory, May 1970; ASTM STP 484, ASTM, Philadelphia, Pa., 1971.
21. J.R. Hawthorne, "Further Observations on A533-B Steel Plate Tailored for Improved Radiation Embrittlement Resistance," ASME Second National Congress on Pressure Vessels and Piping, San Francisco, Calif., June 23-27, 1975.
22. G.R. Irwin, "Plastic Net Ligament Analysis," ACRS, Reactor Pressure Vessels: Steel Subcommittee Meeting, Advisory Committee on Reactor Safeguards, Washington, D.C., July 8, 1975.

## Appendix A

### PROCUREMENT OF A533-B AND A302-B STEEL TEST PLATES FOR DYNAMIC FRACTURE TOUGHNESS STUDIES

J.R. Hawthorne

Procurement specifications for the A533-B and A302-B plates were designed, respectively, to secure materials representative of current reactor vessel construction and early reactor vessels now operating. The purchase specifications for the A533-B plate were patterned primarily after those evolved by Chicago Bridge and Iron (CB&I); those for the A302-B plate were developed by NRL, except for heat treatment specifications, which were developed jointly by representatives of NRL, Combustion Engineering (CE), Babcock and Wilcox (B&W), and Lukens Steel Company.\* In developing heat treatment requirements for the A302-B plate, the metallurgical histories of many old production A302-B plates, including the ASTM A302-B reference plate used in reactor surveillance, were reviewed in detail to establish the range of typical heat treatments used for early vessels. The heat treatment selected, based on this range, is considered to be representative.

Purchase specifications for the two plates are summarized in Table A1. In the case of the A302-B plate, a sulfur content in the range of those of early production A302-B plates was desired, and the use of a specific ingot with 0.025% S was specified. In addition, the specifications for the A302-B plate called for the use of a minimum of cross rolling in producing the 6-in. (152-mm) gage, since a maximum difference in directional properties was desired. Chemical compositions of the A533-B and A302-B plates, as given by the mill test report and as determined independently (courtesy B&W) in accordance with EPRI program requirements, are listed in Table A2. The chemical composition of the ASTM A302-B reference plate has been included in Table A2 for comparison with that of the new A302 plate. Note especially the match in sulfur contents. Actual plate heat treatments are outlined in Table 3. Plate austenitizing, quenching, and tempering treatments were conducted by Lukens Steel; the long-term heat treatments for stress relief annealing were performed at NRL. Stress relief annealing was accomplished using a recirculating air furnace after the primary sectioning of the plates (by NRL) by flame cutting. During the stress relief heat treatment, work piece temperatures were monitored continuously with mechanically attached thermocouples.

Table A4 lists mechanical properties information for the two plates (quarter-thickness location) developed and reported by the mill. On the basis of this information, the plates were certified by Lukens as A533 Grade B Class 1 and A302 Grade B, respectively. Note that, in both cases, the test samples were removed from test dropouts taken after the plate was tempered and accordingly were stress relief annealed separately. The "repeat" test results listed in Table A4 refer to a portion of material returned to Lukens in the as-delivered condition.

\*The contributions based on experience by R. Smith (CE), D. Young (B&W), and B. Imle (Lukens) were most helpful in developing the A302-B plate plan.

**Table A1**  
**Summary of Procurement Specifications for**  
**A533-B and A302-B Steel Test Plates**

Specification	Plate 1	Plate 2
ASTM type/grade	A533-B Class 1* (fire box quality)	A302-B† (fire box quality)
Gage	8 in. (203 mm)	6 in. (152 mm)
Pattern size (total)	120 in. × 142 in. (3.0 × 3.6 m) (RD)‡,§	113 in. × 110 in. (2.9 × 2.8 m) min (RD)‡,§
Melt furnace	Electric	Electric
Melt treatment	VIP (vacuum improved, PV quality)	VIP
Melt/slab number	A3220-2	C4076-1A**
Ingot to plate cross rolling	Standard (3:1) cross roll	Minimum — apply cross rolling only to reach pattern requirement
Heat treatment	Lukens procedure LS-102 dtd. 2/21/69, Rev. 16, dtd. 5/17/74  Stress relief tests only 1150° +25° F (621° +14° C) -50° F (-28° C) for 50 hr	1650° ±25° F, (899° ±14° C) 6 hr WQ 1200° ±25° F, (649° ±14° C) 6 hr AC stress relieve tests only  1150° ±25° F, (621° ±14° C) 24 hr, FC to 600° F, AC
Testing	Ultrasonic to ASME Code Section III, Summer 1972, Addendum NB-2532.1 (Lukens Proc. N-0014, dtd. 1/24/72) (ASME Code Case 1338, Alt. 1, 100%)	Ultrasonic to ASME Code Section III, Summer 1972, Addendum NB-2532.1 (ASME Code Case 1338, alt. 1, 100%)
Required properties	RT-NDT temperature shall not exceed +10° F (-12° C)	Plate (longitudinal orientation) shall meet C <sub>v</sub> 30 ft-lb (41 J) at +10° F (-12° C). DW NDT will be performed for information only. Longitudinal and transverse tensile tests shall confirm A302-B plate properties for 1/4 T location.
Marking	Patterns shall be marked to show primary rolling direction and orientation and position relative to prime plate and original.	Patterns shall be marked to show primary rolling direction and orientation and position relative to prime plate and original.

\*ASTM Designation A533-B, Class 1, Book of ASTM Standards, 1972, Part 4, p. 617.

†ASTM Designation A302-B, Book of ASTM Standards, April 1974, Part 4, p. 113, with additional specifications.

‡(RD) primary rolling direction.

§ All pattern edges to be at least 1-T away from any water quenched edge.

\*\*Ingot composition: 0.22 C, 1.40 Mn, 0.025 S, 0.06 Cu, 0.25 Ni, 0.06 Cr, 0.57 Mo.

## NRL REPORT 8006

Table A2  
Chemical Compositions of A533-B and A302-B Steel Plates

Chem. Compos. (wt %)	A533-B-1 (Metl A3220)		A302-B (Melt C4076)		ASTM A-302-B Ref. Plate**	
	Thickness					
	8-3/16 in. (208 mm)		6-3/8 in. (162 mm)		6 in. (152 mm)	
	Analysis					
	*	†	*	†	‡	
C	0.19	0.23	0.21	0.23	0.23	0.24
Mn	1.30	1.31	1.46	1.40	1.42	1.34
P	0.007	0.005	0.010	0.016	0.008	0.011
S	0.007	0.010	0.021	0.025	0.022	0.023
Si	0.26	0.28	0.24	0.24	0.22	0.23
Ni	0.59	0.65	0.23	—	—	0.18
Cr	0.06	—	0.06	—	—	0.11
Mo	0.52	0.57	0.54	0.57	0.54	0.51
Cu	0.057	—	0.059	—	—	0.20
V	0.010	—	0.012	—	—	<0.001
Al $\phi$	0.021	—	0.034	—	—	0.040
Ti	0.001	—	0.008	—	—	0.015
Co	0.015	—	0.012	—	—	—
Cb	0.005	—	0.007	—	—	—
Ta	<0.01	—	0.02	—	—	—
Sn	0.008	—	0.009	—	—	0.037
B	0.003	—	0.0006	—	—	0.0001
Pb	0.001	—	0.004	—	—	—
As	0.001	—	0.004	—	—	—
Zn	0.0001	—	0.00001	—	—	—

\*Courtesy Babcock and Wilcox Co.

†Mill test report of Lukens Steel Co.

‡Mill test report on retest, by Lukens Steel Co.

$\phi$ Total aluminum

\*\*J.R. Hawthorne, "Radiation Effects Information Generated on the AST Reference Correlation-Monitor Steels," ASTM DS-54, American Society for Testing and Materials, Philadelphia, Pa., July 1974

Metric conversion: in.  $\times$  25.4 = mm

Table A3  
Heat Treatment of A-533-B and A302-B Steel Plates

Steel Type	Thickness	Heat Treatment
A533-B-1	8-3/16 in. (208 mm)	<p>by Lukens Austenitized 1625°-1675° F (885°-913° C), held 1 h per in. minimum, water quenched; tempered 1220° F (660° C) held 1 h per in. min, water quenched.</p> <p>by NRL Stress relief annealed 1150° F + 25° C-50° F (612° C + 14° C-28° C) for 32 h; furnace cooled to below 600° F (316° C) at 100° F (56° C) max per h</p>
A302-B	6-3/8 in. (162 mm)	<p>by Lukens Austenitized 1625°-1675° F (885°-913° C), held 1 h per in. minimum, water quenched; tempered 1220° F (660° C) held 1 h per in. min, water quenched.</p> <p>by NRL Stress relief annealed 1150° F ±25° F (621° C ±14° C) for 32 h; furnace cooled to below 600° F (316° C) at 100° F (56° C) max per h</p>

Table A4  
Mechanical Properties of A533-B and A302-B Plates Given by Mill Test Reports\*

Plate	Melt No.	Orient.	Yield Strength (ksi)	Tensile Strength (ksi)	Elong. in 2.0-in. (%)	RT NDT °F (°C)	NDT °F (°C)	C <sub>v</sub> Properties
A533-B-1	A3220	T† T	69.0 72.0	90.0 92.0	27 25	-10(-23)	-10(-23)	(L) 50° F (10° C): 52,58,57 ft-lb 50,50,50 % shear 40,48,48 mils LE -
A302-B: Original test	C4076	T T	84.0 86.5	97.5 100.0	20 20	not determined	not determined	(L) 10° F (-12° C): 40,35,36 ft-lb 30,30,30 % shear 38,34,34 mils LE
Retest		L‡ L	76.7 79.6	95.0 99.1	22 21			(T) 212° F (100° C): 55,54,50, 48,50,50 ft-lb 50 % shear (all tests) 46,50,50 46,44,46 mils LE

\*Based on test specimens stress relieved by heating to 1125°-1175° F (607°- 635° C), held 24 h and furnace cooled

†T = transverse (TL) orientation

‡L = longitudinal (LT) orientation

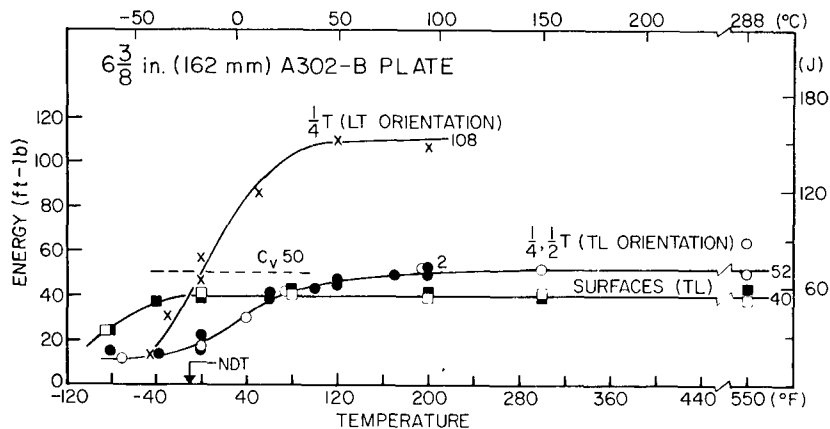
Metric conversion: ft-lb. x 1.356 = J;  
ksi x 6.89 = MPa

**Table A5**  
**Mechanical Properties of A533-B and A302-B Steel Plates After**  
**Stress Relief Heat Treatment by NRL (Preliminary)**

A. Tensile Properties							
Plate	Test Location/ Spec Orientation		75° F (24° C) Yield Strength (ksi)			75° F (24° C) Tensile Strength (ksi)	
A533-B	Top Surface (T.S.), TL Mid-Thickness, TL		69.8 62.6, 63.6			92.8 85.4, 85.6	
A302-B	Top Surface, TL Mid-Thickness, TL		85.4 69.2, 68.9			99.8 89.6, 89.2	
B. Drop Weight NDT							
	NDT Temperature						RT NDT
Plate	T.S.*	1/8 T†	1/4 T	1/2 T	7/8 T†	B.S.*	1/4 T
A533-B	-40° F (-40° C)	0° F (-18° C)	10° F (-12° C)	-10° F (-23° C)	-10° F (-23° C)	-60° F (-51° C)	10° F (-12° C) (DW based)
A302-B	-80° F (-62° C)	-30° F (-34° C)	-10° F (-23° C)	-10° F (-23° C)	-10° F (-23° C)	-90° F (-68° C)	~140° F (60° C) (Cv-based) -10° F (-23° C) (DW-based)
C. Charpy-V Energy Absorption							
Plate		Cv Energy (ft-lb, avg. at 1/4 T)					
		At NDT		At NDT +60° F		At Upper Shelf	
A533-B (NDT = 10° F)		(LT) 54 (TL) 34	85 50		~120 ~95		
A302-B (NDT = -10° F)		(LT) 43 (TL) 17	79 35		108 52		

\*Approximate determination

†Specimens taken 5/8 in. (16 mm) below plate surface

Metric conversion: ksi × 6.89 = MPa;  
ft-lb × .1356 = J

**Fig. A1 — Charpy-V notch ductility of the A302-B steel plate in transverse (TL) and longitudinal (LT) orientations**



## NRL REPORT 8006

Documentation tests of plate properties after the NRL stress relief are currently incomplete. Available data from those tests or test series which have been completed are given in Table A5. Of particular interest, the findings confirm that one objective for the A302-B plate, the development of a low  $C_v$  upper shelf energy level (55 ft-lb, 75 J max) in the transverse (TL) test direction, was in fact achieved by the purchase specifications. The  $C_v$  upper shelf value for the quarter-thickness and midthickness locations was 52 ft-lb, 71 J; the value for the two surface locations was even lower at 40 ft-lb, 54 J. In Fig. A1,  $C_v$  results for the transverse and longitudinal test orientations of the quarter thickness location are indicated. The  $C_v$  upper shelf value for the longitudinal orientation is found to be much higher than that for the transverse orientation (108 vs 52 ft-lb, 146 vs 71 J), consistent with the cross rolling limitations included in the plate specifications. The data for the longitudinal orientation indicate that the requirement of  $C_v$  30 ft-lb (41 J)/min at 10° F (-12° C) was satisfied also.

Drop-weight tests are being conducted to establish the through-thickness NDT temperature gradients in both plates. The data developed thus far indicate that the drop weight NDT temperatures of the A533-B plate and the A302-B plate are, respectively, 10° F (-12° C) and -10° F (-23° C). More importantly, the gradient in NDT temperature for all test locations 5/8-in. (16-mm) below the plate surfaces appears to be 20° F (11° C) max, for both plates. NDT temperatures for the plate surface locations generally are much lower than the NDT temperatures for the quarter-thickness (reference) location. With reference to Figs. 13 and 14 of this report, the observations on NDT gradients and differences are in good agreement with the reported DT toughness determinations.

